

## Structure and Plasticity of Indoleamine 2,3-Dioxygenase 1 (IDO1)

Ute F. Röhrig,\* Olivier Michielin,\* and Vincent Zoete\*

Cite This: *J. Med. Chem.* 2021, 64, 17690–17705

Read Online

ACCESS |



Metrics &amp; More

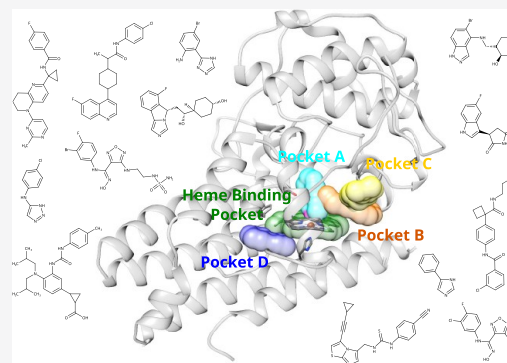


Article Recommendations



Supporting Information

**ABSTRACT:** Since the discovery of the implication of indoleamine 2,3-dioxygenase 1 (IDO1) in tumoral immune resistance in 2003, the search for inhibitors has been intensely pursued both in academia and in pharmaceutical companies, supported by the publication of the first crystal structure of IDO1 in 2006. More recently, it has become clear that IDO1 is an important player in various biological pathways and diseases ranging from neurodegenerative diseases to infection and autoimmunity. Its inhibition may lead to clinical benefit in different therapeutic settings. At present, over 50 experimental structures of IDO1 in complex with different ligands are available in the Protein Data Bank. Our analysis of this wealth of structural data sheds new light on several open issues regarding IDO1's structure and function.



## INTRODUCTION

The heme enzyme indoleamine 2,3-dioxygenase 1 (IDO1) catalyzes the initial and rate-limiting step in the kynurenine pathway of tryptophan metabolism by oxidizing tryptophan (Trp) to *N*-formylkynurenine (NFK) through the addition of molecular oxygen. As a key regulator of immune responses, IDO1 is an important therapeutic target for diseases that involve pathological immune escape, such as cancer.<sup>1,2</sup> Numerous small-molecule IDO1 inhibitors have been published since the discovery of the implication of IDO1 in tumoral immune resistance, and several compounds entered clinical evaluation.<sup>3,4</sup> However, despite compelling preclinical and early clinical data, a phase 3 clinical trial of the IDO1 inhibitor epacadostat in combination with pembrolizumab (ECHO-301) failed to increase the overall and progression-free survival when compared to pembrolizumab alone.<sup>5</sup> Potential reasons for the negative outcome of this clinical trial and possible solutions have been suggested, for example, intratumoral kynurenine level monitoring in combination with the use of more potent and more selective IDO1 inhibitors or dual IDO1–tryptophan 2,3-dioxygenase (TDO) inhibitors.<sup>6,7</sup> Clinical trials with apo-IDO1 inhibitors, having a different inhibition mechanism from epacadostat, are ongoing.<sup>4,8,9</sup>

In addition to its enzymatic activity, IDO1 also displays a signaling activity mediated by two immunoreceptor tyrosine-based inhibitory motifs and a post-transcriptional regulatory site.<sup>2</sup> IDO1's interaction sites with Src homology 2 domain phosphatases (SHPs),<sup>10</sup> phosphoinositide 3-kinases (PI3Ks),<sup>11</sup> and suppressor of cytokine signaling 3 (SOCS3)<sup>12</sup> are all localized in the small domain and are distinct from the enzymatic active site in the large domain (Figure 1A). Novel aspects of IDO1 biology that potentially influence its role as drug target in cancer, infectious diseases, autoimmunity, and

neurodegeneration continue to be discovered, such as its regulation by heme availability,<sup>13</sup> its activation by polysulfides,<sup>14</sup> its nitrite reductase activity,<sup>15</sup> its involvement in the redox signaling pathways of hydrogen peroxide and singlet oxygen,<sup>16,17</sup> and its reactive oxygen species scavenging activity.<sup>18</sup> Therefore, there is an ongoing interest in IDO1's biology and pharmacological inhibitors capable of modulating these different pathways and processes.

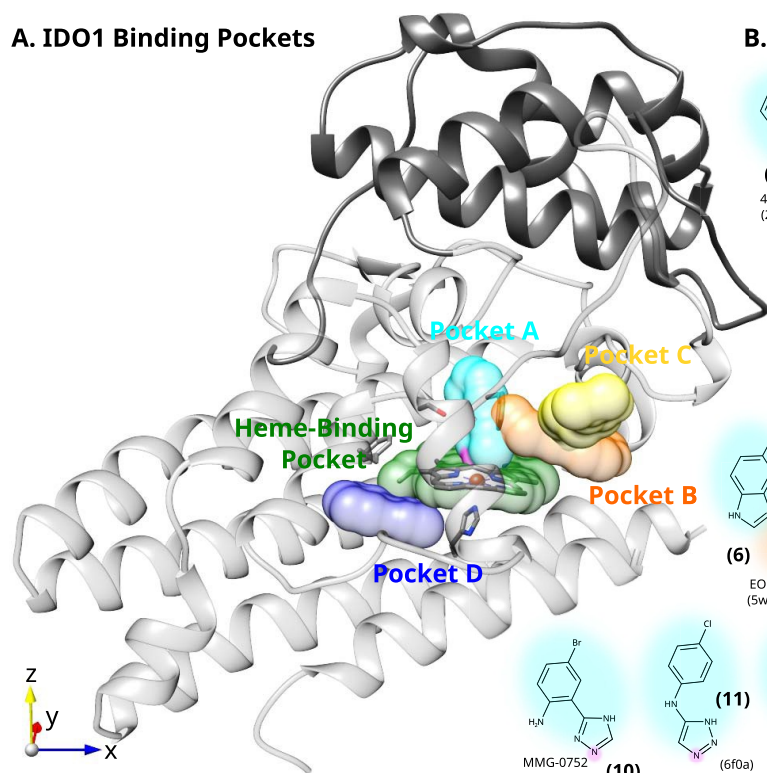
More than 50 crystal structures of IDO1 have been published over the last 15 years, starting with the seminal structure of 4-phenylimidazole-bound IDO1.<sup>19</sup> These structures display a large diversity with respect to bound cofactors and ligands, including the clinical-stage IDO1 inhibitors epacadostat (INCB024360, Figure 1, compound 4),<sup>20</sup> navoximod (NLG-919/GDC919, 3),<sup>21</sup> linrodostat (BMS-986 205, 18),<sup>22</sup> and EOS200271<sup>23</sup> (formerly PF-06 840 003, 6). These structures have yielded a wealth of information and have been used extensively for structure-based drug design.<sup>24</sup> In 2018, the first structures of inhibitor-bound apo-IDO1 were published,<sup>13,25</sup> suggesting that heme binding to IDO1 is reversible under physiological conditions and solving the riddle of how some previously patented compounds from Curadev, Bristol-Myers Squibb, and Flexus Biosciences fit into the IDO1 active site.<sup>26</sup> X-ray structures also supported the classification of IDO1 inhibitors into four types,<sup>27</sup> according to their preferential binding to (i) oxygen-bound holo-IDO1, *e.g.*, 1-methyl-L-

Received: September 24, 2021

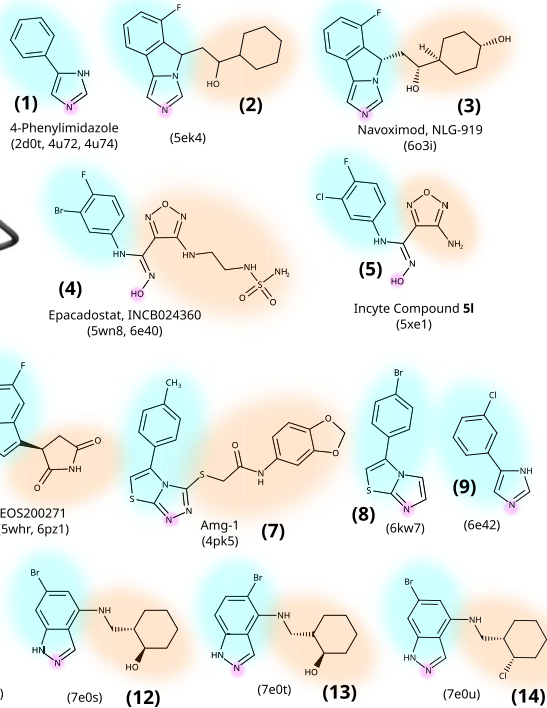
Published: December 15, 2021



## A. IDO1 Binding Pockets



## B. Holo-IDO1 Inhibitors



## C. Apo-IDO1 Inhibitors

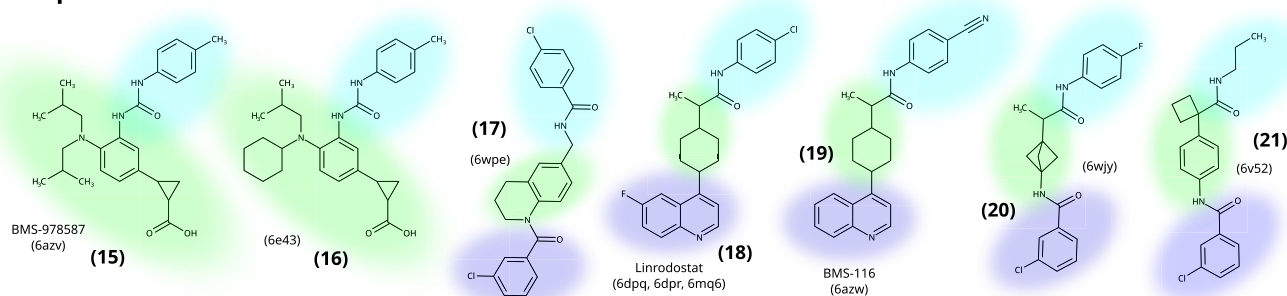


**Figure 1.** IDO1 structure and chemical structures of selected cocrystallized inhibitors. (A) Binding pockets and domains. Pocket A (cyan), pocket B (orange), pocket C (yellow), pocket D (blue), and the heme-binding pocket (green). The site of the iron-binding atom is marked in magenta. The small domain is shown in dark gray ribbons, and the large domain in light gray ribbons. (B) Holo-IDO1 type ii and type iii inhibitors. (C) Apo-IDO1 (type iv) inhibitors. PDB IDs are given in parentheses. The same color code as that in part A is used to designate moieties binding to specific pockets. The chemical structures of all cocrystallized ligands can be found in the [Supporting Information](#) (Figure S1).

tryptophan; (ii) free ferrous holo-IDO1, *e.g.*, epacadostat; (iii) free ferric holo-IDO1, *e.g.*, navoximod; and (iv) apo-IDO1, *e.g.*, linrodostat.

Four subpockets have been defined in the IDO1 active site around the heme cofactor.<sup>27–30</sup> Pocket A<sup>28</sup> (Figure 1A, cyan) is a hydrophobic pocket on the distal heme side, with Ser167 as the main hydrogen bonding partner. Its size and accessibility depend on the conformation of residues 261–265. This pocket seems to be quintessential for inhibitor binding as it is filled by all inhibitors with a known binding mode (Figure 1B, moieties binding to pocket A are marked with a cyan background). Pocket B<sup>28</sup> (Figure 1A, orange) is located toward the entrance of the active site and is only accessible when the flexible JK-loop (residues 360–380, Figure 2) is in an open conformation. It is only filled by larger inhibitors and has not been shown to be occupied by type iv inhibitors (Figure 1C). Its influence on inhibitor affinity seems to be less pronounced than pocket A, which makes it interesting for the modulation of other

compound properties such as absorption, distribution, metabolism, and excretion (ADME). Moieties in this solvent-exposed pocket may also allow the attachment of visual probes, bispecific inhibitors, or proteolysis targeting moieties.<sup>3</sup> Pocket C<sup>30</sup> (Figure 1A, yellow) comprises a surface at the entrance of the active site, which is also occluded by JK-loop closure and has been postulated to interact with some inhibitors based on docking predictions.<sup>31,32</sup> However, in experimental structures pocket C, which has also been called “Sa\* site”, has rarely been found to interact with ligands besides buffer molecules except in cases of the loosely bound conformations of linrodostat and substrate L-Trp after photolysis.<sup>33,34</sup> Pocket D<sup>27</sup> (Figure 1A, blue) is a small binding site located on the proximal heme side that is opened by a conformational change of Phe270. In wild-type holo-IDO1, pocket D is isolated from all other binding pockets by the heme cofactor and acts as a secondary binding site for small ligands. In apo-IDO1, it becomes connected to the other pockets by the absence of heme and is filled by most type iv inhibitors (Figure

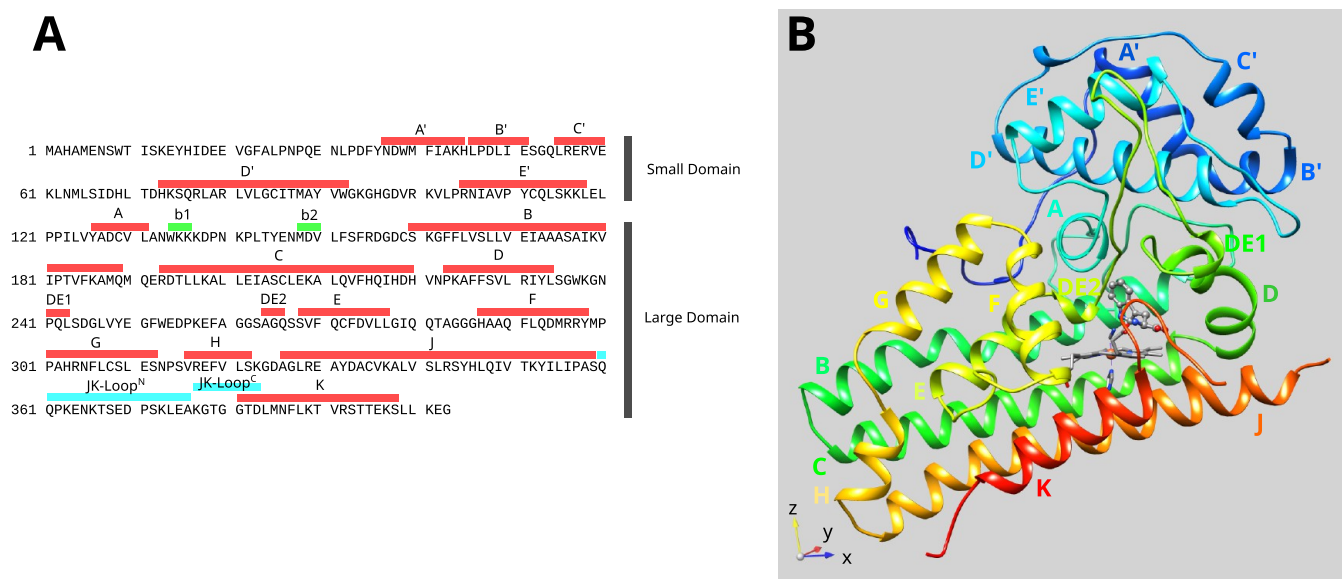


**Figure 2.** Secondary structure elements of IDO1. (A) Human IDO1 sequence (Uniprot ID P14902). The small domain comprises residues 1–120, and the large domain comprises residues 121–403. Helices are marked in red, and  $\beta$ -strands are marked in green. Residues 381–383 are part of either the JK-loop (cyan) or helix K depending on the bound ligand. The novel small helices in the DE connection are called DE1 (241–243) and DE2 (264–266). (B) Secondary structure elements mapped onto the IDO1 structure (PDB ID 5wmu).<sup>29</sup>

1C). This pocket was also suggested to be an inhibitory substrate binding site and was called the “Si site”.<sup>29</sup> Here, we additionally define a “heme-binding pocket” (Figure 1A, green) lined by, among others, the side chains of His346, Val170, Phe214, and Ile217. These residues interact with the heme cofactor in holo-IDO1 and with the central moieties of type iv ligands in apo-IDO1 (Figure 1C).

Open questions remain regarding IDO1’s structure and mechanism, such as (i) the plasticity of the active site in response to bound ligands and redox changes, (ii) the function and conformations of the JK-loop opening or closing the active site, (iii) the presence and function of a channel leading to the active site between helices E and F, (iv) the accessibility of different active site pockets (A, B, C, and D) depending on IDO1 conformations and their role in inhibitor binding, (v) the origin of the observed substrate inhibition at high L-Trp concentrations, (vi) the failure of classical docking codes to provide good predictions for holo-IDO1 inhibitors, and (vii) whether heme binding to IDO1 is reversible and if apo-IDO1 inhibitors bind reversibly or irreversibly.

Here, we contribute to clarifying these issues based on a detailed analysis of the available structural data. We also assess the quality of all structures globally and focused on their ligand binding sites, giving helpful insights for future structure-based drug design studies.

## RESULTS AND DISCUSSION

To date (September 23, 2021), there are 58 structures of IDO1 (Supporting Information, Table S1) available in the Protein Data Bank (PDB),<sup>35</sup> which display a large diversity with respect to bound cofactors and ligands (Table S2). All of them have been determined by X-ray crystallography, and there are no NMR or electron microscopy structures available. Besides six structures with mutations close to the active site (PDB IDs 4u72, 4u74, 5wmu, 5wmx, 6cxu, and 6cxv),<sup>29,36</sup> there are seven ligand-free holo-IDO1 structures (PDB IDs 6azu, 6dpq chain A, 6dpr-A, 6e44, 6e45, 6mq6-A, and 7a62),<sup>13,25,33,37</sup> three with cyanide

and substrate L-Trp (PDB IDs 5wmu, 5wmu, and 6e35),<sup>29</sup> 11 with imidazole inhibitors (PDB IDs 2d0t, 4pk6, Sek2, Sek3, Sek4, 6e42, 6kof, 6kps, 6kw7, 6o3i, and 7m7d),<sup>19,25,38–41</sup> six with triazole inhibitors (PDB IDs 4pk5, 6f0a, 6r63, 7ah4, 7ah5, and 7ah6),<sup>27,38,42</sup> six with indazole inhibitors (PDB IDs 7e0o, 7e0p, 7e0q, 7e0s, 7e0t, and 7e0u),<sup>43</sup> five with hydroxyamide inhibitors (PDB IDs 5wn8, 5xe1, 6e40, 6e41, and 6pu7),<sup>25,29,44,45</sup> and two with the indole inhibitor EOS200271 (PDB IDs 5whr and 6pz1).<sup>23,46</sup> In addition, there are eight heme-free apo-IDO1 structures bound to type iv ligands (PDB IDs 6azv, 6azw, 6e43, 6v52, 6wjy, 6wpe, 6x5y, and 7m63)<sup>13,25,33,41,47–50</sup> and three partially heme-free structures (PDB IDs 6dpq-B, 6dpr-B, 6mq6-B).<sup>33</sup>

Secondary structure elements have first been visually defined for IDO1 (helices A–S)<sup>19</sup> and later in comparison with TDO (helices A–K),<sup>51</sup> thereby neglecting the small domain. The latter naming is predominant in the recent literature and has been complemented by denoting the helices in the small domain as A’–E’.<sup>25</sup> Here, we preserve this convention and define helices A’–E’ in the small domain and helices A–K in the large domain based on the available structural data (Figure 2). We found two new small helices in the long loop connecting helices D and E, which we called helix DE1 and DE2. To compare the active site structures of all available complexes, we superimposed each protein chain with chain A of the cyanide- and L-Trp-bound structure 5wmu,<sup>29</sup> which is of good quality and probably resembles the enzymatically active state, taking into account only the backbone of helices B, C, H, J, and K of the large domain. For the discussion and all figures, we oriented the reference structure in such a way that the C $\beta$  and C $\delta$  atoms of the heme lay approximately on the x-axis (front and back of the active site, blue axis in Figure 1), the C $\alpha$  and C $\gamma$  atoms of the heme lay on the y-axis (left and right of the active site, red axis), and the His346–iron bond lay on the z-axis (up and down, yellow axis).

**Structure Quality Assessment.** It is often assumed that structural models deposited in the PDB are of equally high quality or that their quality only depends on the resolution.

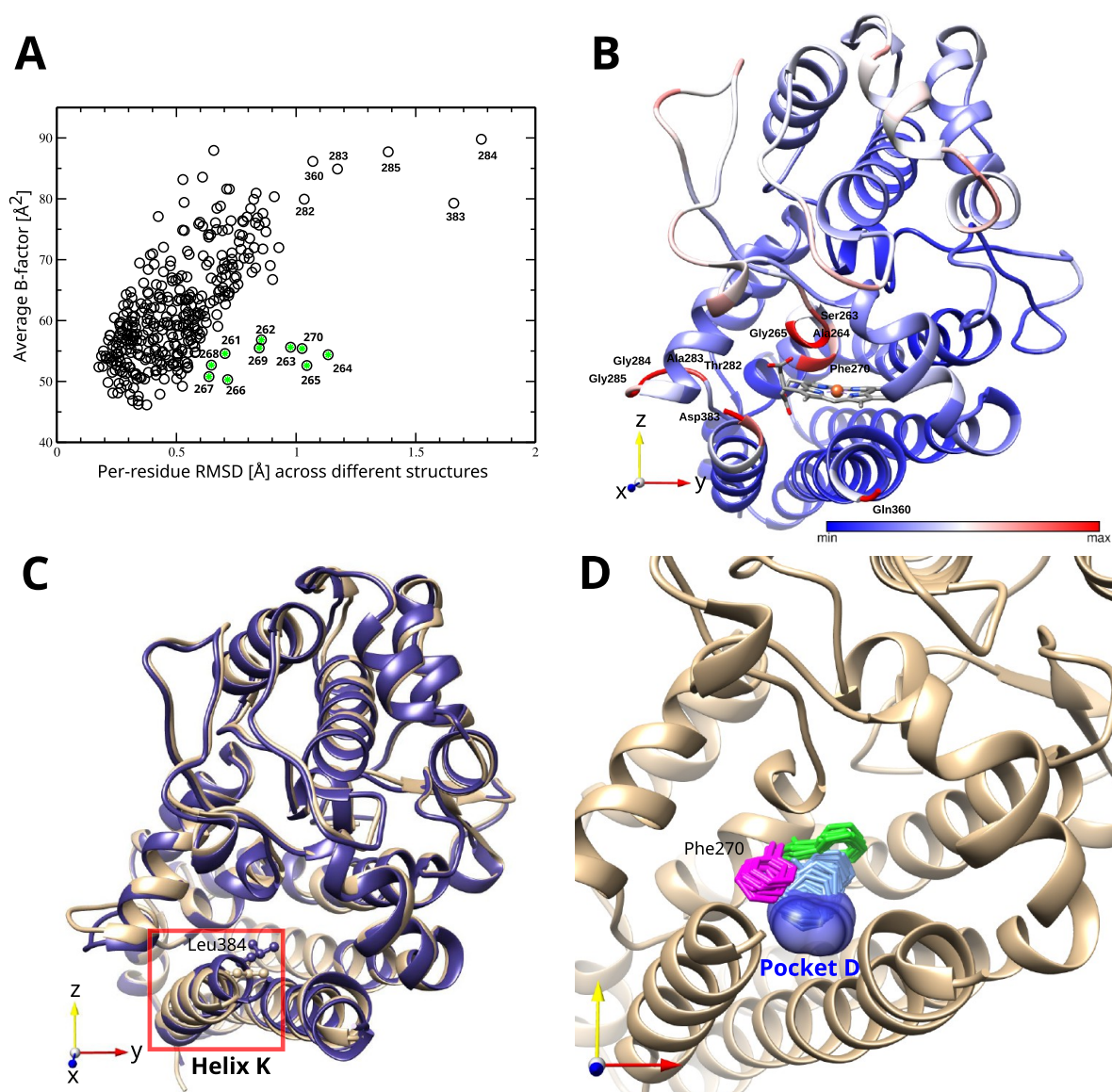


**Figure 3.** Structural flexibility. (A) Correlation between the per-residue backbone rmsd of different IDO1 X-ray structures and the average per-residue B-factors. The residue numbers of outliers are given, and outliers with a high rmsd but a low average B-factor are marked in green. (B) Average IDO1 structure, colored as a function of the rmsd. The heme cofactor is colored by the atom type and displayed to indicate the active site. (C) Position of helix K in apo-IDO1 (purple, 6wjy) as compared to holo-IDO1 (tan, 6e42), highlighting the position of Leu384. (D) Conformations of Phe270 in apo-IDO1 (magenta), holo-IDO1 without a pocket D ligand (light blue), and holo-IDO1 with a pocket D ligand (green). Pocket D is shown as a blue surface.

However, these models are based on an interpretation of experimental data. One tool to globally assess the quality of a structural model is the wwPDB Structure Validation Report.<sup>52,53</sup>

The results of this assessment are visually summarized on the PDB access sites of each X-ray structure by comparing five parameters (*R*-free value, clashscore, Ramachandran outliers, side chain outliers, and real-space *R*-value *Z*-score outliers) with the average values of all deposited X-ray structures. Together with the resolution and the atomic *B*-factors, also called temperature factors or atomic displacement parameters, these values give an indication of the quality of a model. Another tool is the diffraction-component precision index (DPI),<sup>54,55</sup> which measures the uncertainty of the atomic coordinates of the 3D model. Here, we report for each IDO1 structural model its resolution, its *R*-free value, and its DPI (Supporting Information, Table S1). Seven IDO1 models have a DPI larger than 0.8 Å and

therefore a high global coordinate uncertainty (PDB IDs 2d0u, 4pk6, 5xe1, 6azv, 6azw, 7e0o, and 7m63).

However, more important in the context of structure-based drug design is the local structure quality at the ligand binding sites. Specific tools have been developed for this purpose, for example, the Validation Helper for Ligands and Binding Sites (VHELIBS)<sup>56</sup> and the Electron Density Support for Individual Atoms (EDIA) as well as its extension for multiple atoms (EDIAM).<sup>57</sup> Here, we computed the VHELIBS classification, EDIAM value, and average *B*-factor for each ligand of interest. The values for the heme-pocket ligands, the iron-bound ligands, the A-pocket ligands, and the D-pocket ligands are reported in Tables S2 and S3. A ligand with a *B*-factor above 100 Å<sup>2</sup> is considered to be significantly disordered, and a ligand with an EDIAM value below 0.4 is considered to show substantial inconsistencies with the electron density fit. We marked the

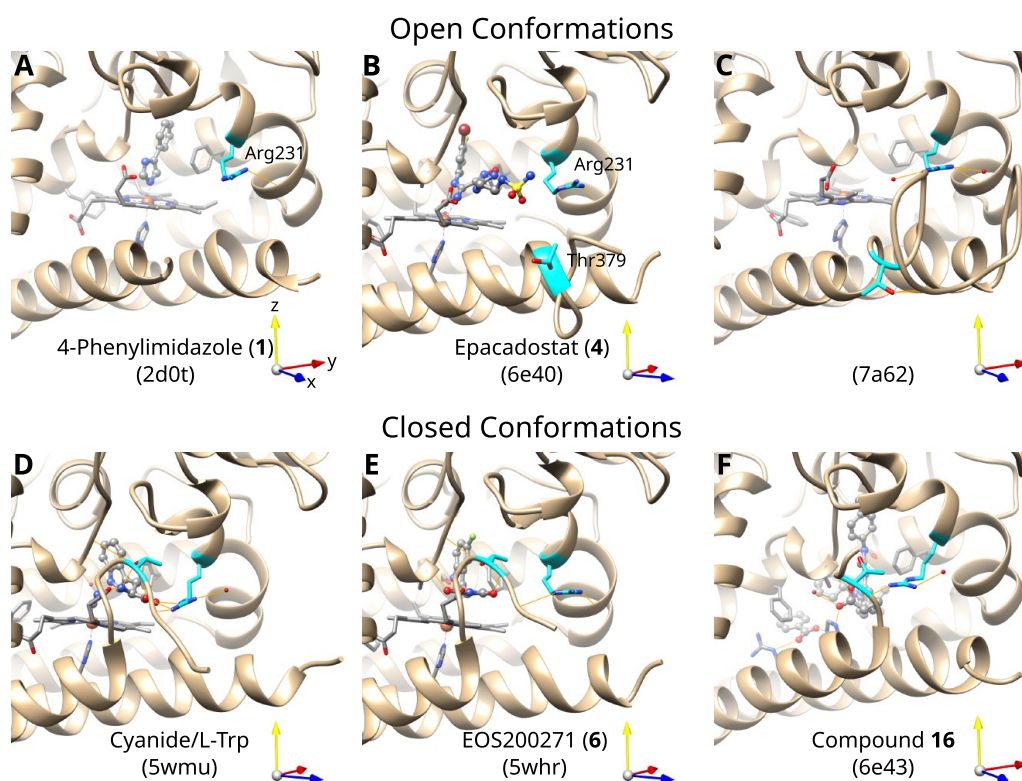


**Figure 4.** JK-loop<sup>C</sup> conformations. Residues Thr379 and Arg231 are highlighted in cyan, and their hydrogen bonding network is shown by thin orange lines. (A–C) Holo-IDO1 with open JK-loop<sup>C</sup> conformations. (D and E) Holo-IDO1 with closed JK-loop<sup>C</sup> conformations. (F) Apo-IDO1 with partially closed JK-loop<sup>C</sup> conformation. Additional conformations are shown in Figure S2.

ligands that failed one of these filters in red in Table S2. The VHELIBS analysis additionally yields information about the quality of the ligand binding site (Table S3). In the following, we focus our discussion on higher-confidence models when multiple models with similar ligands are available.

Models with a high global coordinate uncertainty and models with significantly disordered ligands should be used with caution, for example, in structure-based drug design studies. In the following, we will refer to structural models as structures in agreement with common practice, keeping in mind that both the underlying experimental data and its interpretation can be of varying quality.

**Structural Flexibility.** To distinguish the structural flexibility in response to bound ligands and cofactors from thermal motions of intrinsically flexible loops, we structurally aligned all IDO1 X-ray structures (apo and holo) and calculated the root-mean-square deviation (rmsd) of the backbone of each residue from its average position as well as the average *B*-factor for each residue. Residues located in flexible loops should simultaneously display high rmsd values and high *B*-factors, while residues with well-defined but distinct positions in different structures should display high rmsd values but low *B*-factors (Figure 3A). The results of this analysis show that residues 282–285 in the EF-loop (Figure 2) and residues 360–383 in the JK-loop (mainly unresolved because of this flexibility) fit the first category. On the other hand, residues 261–270 close to the active site fit the second category, having a high rmsd but a low *B*-factor. These residues, which belong to the C-terminal part of the DE-loop, helix DE2, and the N-terminal part of helix E, thus adopt different positions in response to different ligands and potentially also in response to different heme oxidation states. For residues 260–265, the role of providing flexibility was

already postulated in 2006 based on their highly conserved and glycine-rich sequence (AGGSAG).<sup>19</sup> We will discuss the different positions and conformations of these residues and their impact on the size and shape of pocket A throughout this work.

Apo and holo-IDO1 structures are very similar, with an average backbone rmsd of 0.6 Å. However, the N-terminus of helix K is in a slightly different position, with Leu384 moving into the space freed by the absence of heme in apo-IDO1 (Figure 3C). Besides this region, the largest structural difference between apo and holo structures concerns Phe270, which adopts a conformation in the apo structures that would clash with the heme cofactor in the holo structures and that closes the solvent channel between helices E and F (Figure 3D). Pocket D, as defined for the holo structures, is filled by all apo-IDO1 ligands, with the exception of one structure (PDB ID 6azv).

**JK-Loop Structure.** In most IDO1 structures, the JK-loop is unresolved because of its flexibility, and the N terminus of helix K starts around residue Thr382 (Figure 4A). This loop has been divided into a highly disordered and solvent-exposed N-terminal part comprising residues 360–376 (JK-loop<sup>N</sup>) and a C-terminal part comprising residues 377–383 (JK-loop<sup>C</sup>).<sup>58</sup> In structures of the K116A/K117A double mutant, which was developed to generate new crystal forms by reducing the surface entropy to obtain high-resolution diffraction data,<sup>25</sup> helix K is extended on its N terminus, already starting around residue Thr379 (Figure 4B). All these structures can safely be assumed to have an open loop conformation because in a closed conformation there would be specific contacts that would reduce flexibility and make the electron density more visible. They probably represent the resting state of the ligand-free holo enzyme, which is then perturbed by substrate or inhibitor binding. This assumption is

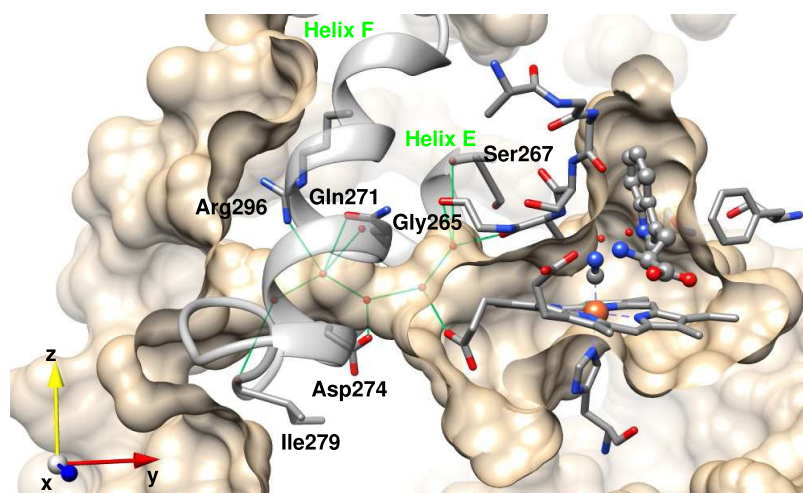


**Figure 5.** IDO1 water and oxygen channel structure, shown for the cyanide- and *L*-Trp-bound complex (PDB ID 5wmu). The hydrogen bonding network of the solvent molecules inside the channel is highlighted by thin green lines.

supported by the only structure with a completely resolved JK-loop (PDB ID 7a62-C, Figure 4C).<sup>37</sup> Although the loop residues have a poor electron density and very high *B*-factors (150 Å<sup>2</sup>), they clearly show an open conformation for the ligand-free ferrous holo-IDO1 structure.

In the substrate (*L*-Trp) bound structures (PDB IDs 5wmu, 5wmv, 6e35, and 6e46),<sup>25,29</sup> JK-loop<sup>C</sup> is always resolved. Here, helix K is shorter with respect to the ligand-free state, and residues 377 to 383 form a bulge that closes the active site and is stabilized by numerous hydrogen bonds (Figure 4D). At the same time, the side chain of Arg231, which has been shown to be important for the enzymatic activity of IDO1,<sup>19</sup> flips inward to form both a salt bridge with the carboxylate group of the *L*-Trp substrate and a hydrogen bond to the backbone of the JK-loop residue Lys377. Interestingly, the same loop conformation is present in the amino-triazole (**11**) bound structure (PDB ID 6f0a)<sup>42</sup> where, in addition to the inhibitor, a free *L*-Ala is bound to IDO1, mimicking the amino acid function of the *L*-Trp substrate by making the same interactions (Supporting Information, Figure S2A). It was shown by the authors of this structure that the presence of free alanine improves the IC<sub>50</sub> value of the inhibitor for IDO1 5- to 10-fold,<sup>42</sup> suggesting that the active site closure by the bulge is beneficial for its binding affinity. In the EOS200271 (**6**) bound structures (PDB IDs 5whr and 6pz1),<sup>23,46</sup> the active site is also closed, and the loop makes similar interactions but adopts a slightly different conformation as the succinimide group is smaller than the *L*-Trp backbone. Additionally, Arg231 cannot form a salt bridge with the ligand and remains flipped out in a solvent-exposed position (Figure 4E). Yet another distinct closed loop conformation is present in the complex of IDO1 with an indazole compound (**14**, PDB ID 7e0u).<sup>43</sup> Here, the loop is pushed aside by the B-pocket extension of the ligand, which nevertheless makes hydrophobic interactions with Gly378 and Thr379 (Figure S2B).

In most apo-IDO1 structures, JK-loop<sup>C</sup> is unresolved and therefore probably also in an open conformation. One structure (compound **16**, PDB ID 6e43) is the exception,<sup>25</sup> where the loop is resolved starting from Ala376 and displays a partially closed conformation (Figure 4F). This conformation is distinct from all loop conformations seen in the holo structures and does not directly interact with the ligand.

In summary, the JK-loop is highly flexible and can adopt distinct conformations in response to bound ligands. In ligand-free holo-IDO1, JK-loop<sup>C</sup> seems to prefer an open conformation, showing little interaction with heme. Only ligands of a specific size and polarity, mimicking those of *L*-Trp, have been shown to be stabilized by interactions with this loop. Smaller ligands cannot stabilize a closed-loop conformation, while larger ligands occupy all of pocket B and impede loop closure. Therefore, JK-loop interactions contribute to the binding affinity of only a small part of IDO1 inhibitors. So far, no apo-IDO1 inhibitor has been shown to interact with the JK-loop.

**Solvent and Gas Channel.** The channel leading from the protein surface to the heme that passes between helices E and F (Figure 5) was first described in 2017,<sup>29</sup> although it was also present in earlier X-ray structures. This channel is open in most holo-IDO1 structures except for the ligand-free ferric IDO1 structures with Ala264 bound to the heme iron (PDB IDs 6azu and 6e44-A/C), where an inward movement of helix E diminishes its size. Due to its size and occupation by water molecules in higher-resolution structures, it is safe to assume that this channel provides access for water and also probably O<sub>2</sub> to the active site. The substrate *L*-Trp and the heme cofactor, on the other hand, are more likely to enter the active site through the larger opening provided in the ligand-free state by the opened JK-loop (Figure 4A). In apo-IDO1, the channel is generally closed by the side chain conformation of Phe270.

**Ligand-Free and Substrate-Bound Holo-IDO1.** Holo-IDO1 exists in two oxidation states, a ferric state with a net charge of  $-1$  and a ferrous state with a net charge of  $-2$  on the heme cofactor, substantially influencing the electrostatics in the highly hydrophobic active site. While the reduced state is the enzymatically active state, the ferric state is prevalent both under aerobic *in vitro* conditions and in crystallographic studies. The reductant sodium dithionite has been used to obtain ferrous IDO1 after protein crystallization, therefore potentially hindering larger structural rearrangements.<sup>25,37</sup> The two X-ray structures of free ferrous IDO1 (PDB IDs 6e45 and 7a62),<sup>25,37</sup> and the five structures of free ferric IDO1 (PDB IDs 6azu, 6dpq-A, 6dpr-A, 6e44, and 6mq6-A)<sup>13,25,33</sup> generally show very few structural differences (backbone rmsd <0.5 Å). In all structures, residues 261–265 on one side and Phe163 on the other side are in proximity and close access to pocket A in the distal heme site (Figure 6A). However, there are two distinct conformations of

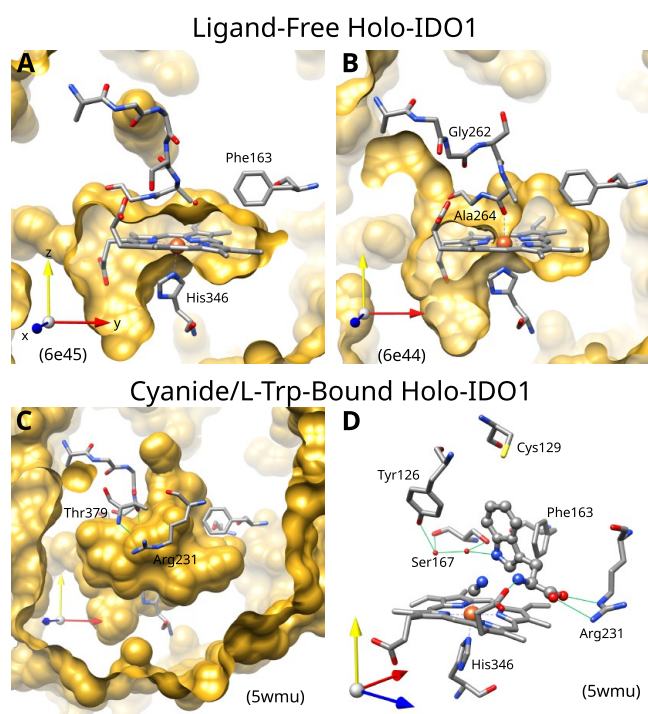


**Figure 6.** Holo-IDO1 active site structures. Hydrogen bonds are shown as thin green lines. (A) Ferrous ligand-free form with a closed A pocket (PDB ID 6e45). (B) Ferric ligand-free form with Ala264 bound to heme iron and a closed A pocket (PDB ID 6e44). (C) Cyanide–L-Trp bound structure (PDB ID 5wmv). The active site is closed off from the solvent by the movement of Arg231 and the JK-loop<sup>C</sup>, forming hydrogen bonds with L-Trp through Thr379. (D) The same structure as that shown in part C showing details of cyanide and L-Trp binding. Thr379 is omitted for clarity.

residues 261–265. In all ferrous structures and five of the 11 ferric IDO1 chains (PDB IDs 6dpr-A, 6dpr-A, 6e44-B/D, and 6mq6-A), residues 261–265 adopt a similar backbone conformation as that in the ligand-bound structures (Figure 6A). In the other six ferric IDO1 chains (PDB IDs 6azu-A–D and 6e44-A/C), the backbone amide oxygen of Ala264 is bound to the heme iron, which is accompanied by a backbone rearrangement of Gly262 (Figure 6B). It is unclear which one of the two conformations observed in the ferric state is prevalent under physiological conditions and if the observed structural changes are due to heme oxidation or different crystallization conditions.

The three cyanide- and L-Trp-bound structures (PDB IDs 5wmv, 5wmv, and 6e35)<sup>29</sup> probably resemble the enzymatically active state most closely despite their ferric oxidation state, with the cyanide mimicking the dioxygen. In these complexes, access to the active site is closed by the JK-loop<sup>C</sup> and a flip of the Arg231 side chain (Figure 6C, see discussion above). Residues 261–265 and Phe163 are pushed apart in the *y*-direction with respect to the ligand-free state. The indole ring of L-Trp, which is sandwiched between Ala264 and the perpendicular aromatic side chain of Phe163 (Figure 6C and D), is perpendicular to the heme plane but off-center in *y*-direction, probably in an optimal conformation to react with iron-bound dioxygen. Besides hydrogen bonds with Thr379 of JK-loop<sup>C</sup> and a salt bridge with Arg231 at the entrance of the active site, L-Trp forms another salt bridge between its amino function and one heme propionate. In the back of the active site, L-Trp forms hydrogen bonds with Ser167 and Tyr126 bridged by two water molecules

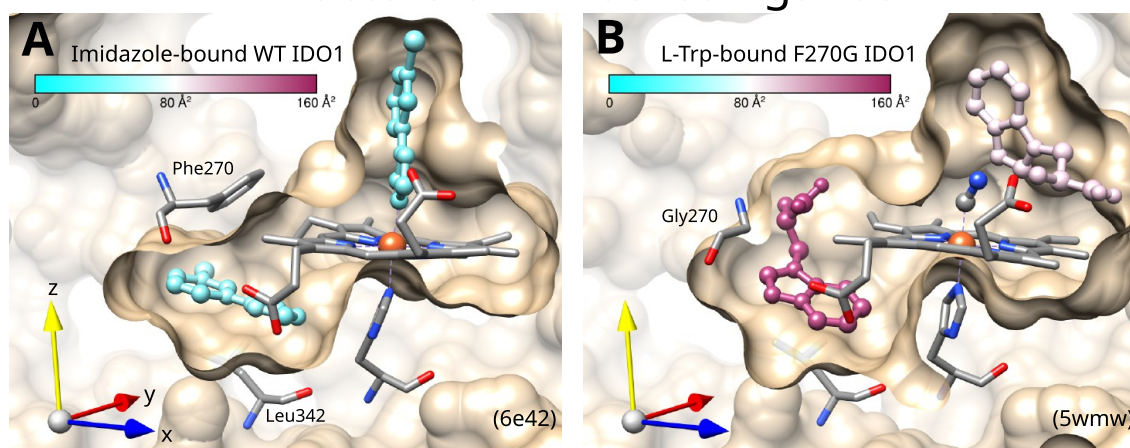
(Figure 6D). In the reduced state and the absence of cyanide (6e46),<sup>25</sup> L-Trp binds in a similar fashion. However, its indole ring is slightly rotated, with loop 262–265 and Phe163 moving inward and narrowing the sandwich structure. In summary, the active site seems to be optimally suited to accommodate L-Trp by providing a largely hydrophobic environment for the indole ring on the one hand and hydrogen bonding partners and charge-neutralizing groups for all of its polar functions on the other hand.

To sum up, it is not completely clear if redox changes in the heme cofactor induce structural changes in the active site. If they exist, they seem to be confined to the structure of residues 261–265. However, L-Trp binding clearly induces major structural changes in the active site, opening pocket A and closing JK-loop<sup>C</sup>, thereby closing or reducing the sizes of pockets B and C.

**Pocket D and Substrate Inhibition.** There are three main hypotheses for the observed substrate inhibition of IDO1, which causes reduced enzyme activity at high L-Trp concentrations.<sup>59–61</sup> At present, the wealth of structural data available for IDO1 allows for a re-evaluation of these hypotheses.

- The inhibitory binding site hypothesis. This hypothesis evokes a second inhibitory L-Trp binding site  $S_p$ ,<sup>61–64</sup> which has later been suggested to be located at the heme proximal site<sup>29,36</sup> coinciding with pocket D. In holo-IDO1, pocket D is opened by a conformational change of the side chain of Phe270 and can accommodate 3-indoleethanol (PDB ID 5wmv),<sup>29</sup> halogen-substituted phenyl azoles (PDB IDs 6e42, 6r63, 7ah4, 7ah5, and 7ah6),<sup>25,27,65</sup> and EOS200271 (6, PDB ID 6pz1)<sup>46</sup> at the high ligand concentrations used in crystallization experiments (Figure 7A). It can be classified as a secondary binding site as it has never been found bound to a ligand when pocket A is empty. L-Trp binding to pocket D has only been observed when a F270G mutation (PDB ID 5wmv) was introduced,<sup>29</sup> significantly increasing the size of this pocket by replacing a benzyl group with a hydrogen atom (Figure 7B). The average *B*-factor of the D-pocket bound L-Trp is very high (135–146 Å<sup>2</sup>), and the EDIAM value is extremely low (0.05–0.06) in both protein chains, indicating a high coordinate uncertainty based on a low electron density. For comparison, when soaking IDO1 crystals with a 20 mM solution of ligand 9 (PDB 6e42), this ligand binds not only to pocket A (*B*-factor of 34 Å<sup>2</sup>, EDIAM value of 1.00) and pocket D (*B*-factor of 38 Å<sup>2</sup>, EDIAM value of 0.98) but also to low-affinity sites on the surface of the protein.<sup>25</sup> However, under similar conditions (crystal soaking with a 25 mM solution of L-Trp) there is no structural evidence of L-Trp binding to pocket D in the wild-type ferrous protein (PDB ID 6e46).<sup>25</sup> This finding also undermines the hypothesis that L-Trp was never observed in pocket D in wild-type IDO1 because its affinity for this pocket was lower in the ferric state than in the ferrous state.<sup>29</sup> We conclude that available structural data do not support the hypothesis that pocket D is a L-Trp binding site that leads to inhibition.
- The ordered binding and blocked access hypothesis. The second hypothesis suggests that bound L-Trp prevents molecular oxygen from approaching the heme iron.<sup>66</sup> While it is true that L-Trp binding induces a closing of the active site through conformational changes of JK-loop<sup>C</sup> and Arg231 as discussed above, the water and gas channel

## B-Factors of D-Pocket Ligands



## Electrostatic Potential of Ferrous IDO1

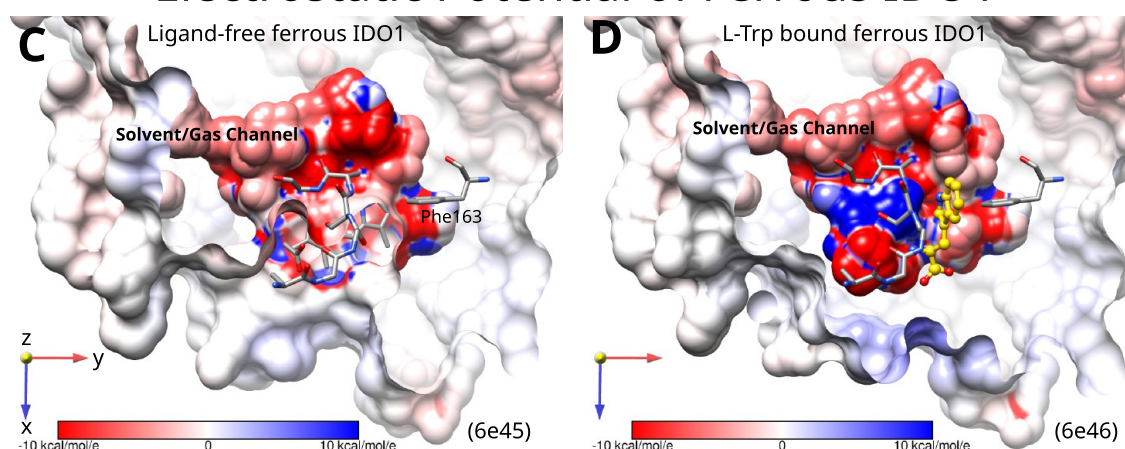


**Figure 7.** Substrate inhibition hypotheses. (A and B) D-pocket ligands colored by their atomic B-factors. (A) Ligand 9 in WT IDO1. The average B-factor of the D-pocket ligand is  $38 \text{ \AA}^2$  (PDB ID 6e42-A). (B) L-Trp in the F270G mutant IDO1. The average B-factor of the D-pocket ligand is  $147 \text{ \AA}^2$  (PDB ID 5wmw-B). Pocket D is substantially bigger in the mutant structure, and the electron density for the second L-Trp is weak. (C and D) Electrostatic potential in the IDO1 active site in the ferrous state, top view along z-axis. Only residues 261–265 and Phe163 are shown for clarity. (C) Ligand-free structure (PDB ID 6e45). (D) L-Trp bound structure (PDB ID 6e46). L-Trp binding induces a positive potential at the heme iron, which increases the reduction potential and hinders  $\text{O}_2$  binding.

passing between helices E and F and leading to the heme is open both in the ligand-free ferrous IDO1 structure (PDB ID 6e45) and in the L-Trp bound ferrous IDO1 structure (PDB ID 6e46, Figures 7C and D).<sup>25</sup> Therefore, there is no structural evidence for this hypothesis.

- The ordered binding and reduction potential hypothesis. The third hypothesis attributes substrate inhibition to a slower turnover when L-Trp binds to ferrous IDO1 before  $\text{O}_2$ .<sup>67</sup> This slowdown has further been attributed to modulation of the heme reduction potential by L-Trp binding.<sup>68</sup> Comparing the electrostatic potential (ESP, computational details are given in the Supporting Information) in the active site of the ferrous ligand-free state (PDB ID 6e45) to the ferrous L-Trp bound state (PDB ID 6e46)<sup>25</sup> indeed reveals a striking difference (Figure 7C and D, respectively). In the ligand-free state, the ESP close to the heme iron is strongly negative, while in the L-Trp bound state the ESP at the heme iron is strongly positive. This inversion seems to be mainly induced by the proximity of the positively charged amino group of L-Trp, even though it forms a salt bridge with a

heme propionate. The negatively charged carboxylate group of L-Trp points further away and forms a salt bridge with Arg231. This change in the electrostatic potential should cause an increase of the heme redox potential  $E_m^0$  and render  $\text{O}_2$  binding less favorable, as this step corresponds to an oxidation of the iron ion. The finding of an increased  $E_m^0$  due to L-Trp binding is in good agreement with experimental data<sup>34,68,69</sup> and supports the hypothesis of the heme redox potential being the origin of the observed substrate inhibition in IDO1.<sup>68</sup>

**Holo-IDO1 Type ii and iii Inhibitors.** All cocrystallized holo-IDO1 inhibitors bind to pocket A in the heme distal site, and larger ligands also occupy pocket B (Figure 1B). For some smaller ligands, a second molecule binds to pocket D (Table S2). The solvent and gas channel between helices E and F is open in all structures. JK-loop<sup>C</sup> is mostly in an open conformation, with the exception of three structures (PDB IDs 5whr, 6a0f, and 7e0u; Figures 4 and S2). The cocrystallized holo-IDO1 inhibitors can be divided into three main chemical classes, namely (i) indoles, (ii) hydroxyamidines, and (iii) azoles.

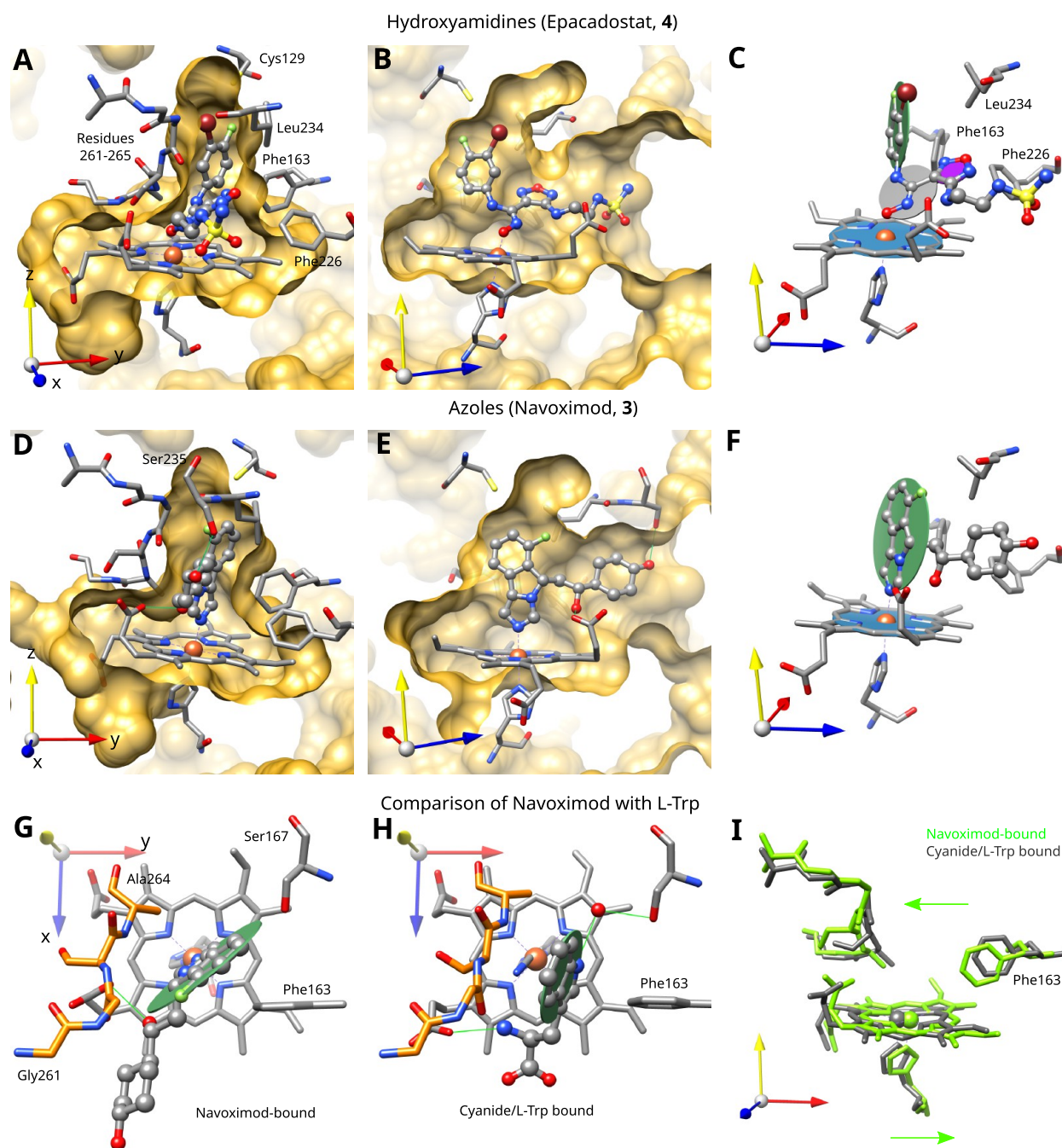


**Figure 8.** Holo-IDO1 type ii and iii inhibitors. Hydrogen bonds are shown as thin green lines. Planar substructures and their orientations are highlighted. (A–C) Epacadostat-bound structure (PDB ID 6e40). (D–F) Navoximod-bound structure (PDB ID 6o3i). (G and H) Top view of the navoximod-bound structure and the cyanide- and L-Trp-bound structure (PDB ID 5wmu). The orientations of the main aromatic planes are shown in green. Residues 261–264 are shown in orange. (I) Active site structure comparison between the cyanide- and L-Trp-bound structure (PDB ID 5wmu, gray) on the one hand and the navoximod-bound structure (PDB ID 6o3i, green) on the other hand.

Of the first class, only the structure of indole EOS200271 (**6**) has been experimentally determined (PDB IDs 5whr and 6pz1).<sup>23,46</sup> EOS200271 is distinguished from all other ligands by not forming a bond to the heme iron and by inducing the closure of JK-loop<sup>C</sup>. Despite its similarity to the substrate L-Trp, the conformation of its indole ring is different (Figure 4D and E). EOS200271 displays an  $IC_{50}$  value of 0.41  $\mu$ M and a ligand efficiency (LE) of  $-0.51$  kcal/mol, which is the highest of any holo-IDO1 inhibitor that binds both to pockets A and B (Supporting Information, Table S4). Apparently, its affinity to IDO1 is driven by interactions with JK-loop<sup>C</sup> and pocket A,

compensating for the absence of a stabilizing iron bond seen in all other holo-IDO1 inhibitors.

In the hydroxyamidine–IDO1 complexes (PDB IDs 5wn8, 5xe1, 6e40, 6e41, and 6pu7),<sup>25,29,44,45</sup> the active site structure is similar to the cyanide- and L-Trp-bound state, but Phe163 and residues 261–265 adapt slightly to the shapes of the inhibitors. The phenyl ring of epacadostat (**4**, PDB IDs 5wn8 and 6e40)<sup>25,29</sup> binds perpendicular to the heme plane (green and blue planes in Figure 8C, 86° angle), while the planar hydroxyamidine function (gray plane in Figure 8C) binds at an angle of 47° to the heme and fits perfectly into the funnel

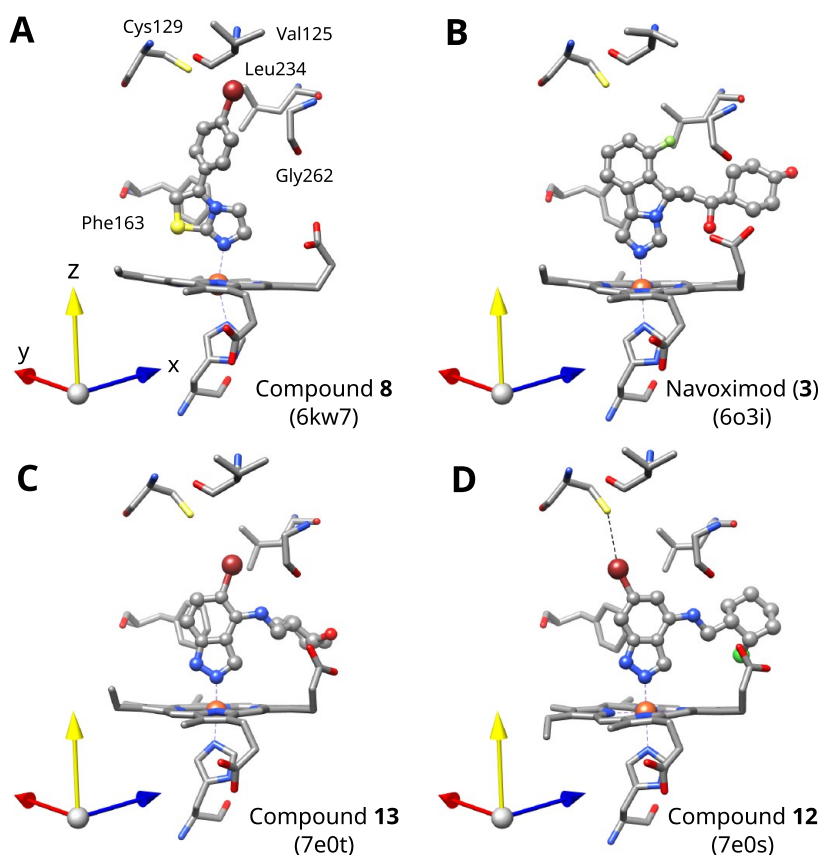


**Figure 9.** Halogen substituents in pocket A. (A) “High position” shown in compound 8. (B) The fluorine position, shown in navoximod (3). (C) “Low position”, shown in compound 13. (D) 6-Substituted indazole (12) with a sulfur–bromine halogen bond.

provided by the backbone of Ala264 and the side chain of Phe163 (Figure 8A–C). The furazan ring of epacadostat (Figure 8C, magenta plane) fits nicely into the space between Gly262 and Ser263 on the left side, Leu234 above, and Phe163 and Phe226 on the right side but does not make any hydrogen bonding interactions. The *N*-ethylsulfamide chain, which extends toward Arg231 in its open conformation and forms a hydrogen bond with it in some structures, experiences fewer steric constraints from the protein (Figure 8B). This binding mode of epacadostat, which was determined independently by two groups,<sup>25,29</sup> is different from the one of the first reported hydroxyamidine structure (5, PDB ID 5xe1)<sup>44</sup> of the Incyte lead compound 5I.<sup>70</sup> In this structure with a high coordinate uncertainty, ligand 5 was assumed to bind through the amidine nitrogen atom to the heme iron, a binding mode that was shown to be in conflict with quantum chemical calculations.<sup>71</sup> Using density functional theory (DFT) calculations to optimize the geometry of ligand 5 bound to a heme model system (Supporting Information, Table S5), we found that only the neutral ligand binds in a conformation close to the one seen in the X-ray structures of epacadostat, with the phenyl ring roughly perpendicular to the heme plane and the amidine group forming an angle of about 40° with the heme plane (Figure 8C). The calculations show that the heme-bound conformation is influenced more by the protonation state of the ligand than by the redox state of the heme iron, supporting the hypothesis that the hydroxyamidines bind to IDO1 predominantly in their neutral form. This is at variance with our earlier findings,<sup>71</sup> which were based on less reliable X-ray data.<sup>44</sup> The IC<sub>50</sub> values of the cocrystallized hydroxyamidine ligands are in a narrow range

between 35 and 73 nM (Table S4). Interestingly, the smaller lead compound 5 (67 nM, PDB ID 5xe1) has the same potency as epacadostat (73 nM, PDB IDs 5wn8 and 6e40), which extends further into pocket B. The LE for 5 (−0.54 kcal/mol) is therefore higher than that for epacadostat (−0.39 kcal/mol); however, epacadostat was optimized for other properties such as oral bioavailability.<sup>20</sup>

In contrast to the hydroxyamidine ligands, the cocrystallized azole ligands (imidazoles, 1,2,3-triazoles, 1,2,4-triazoles, and indazoles) need more space above the heme iron in *z*-direction to bind the azole ring perpendicular to the heme plane. Therefore, the heme and the protein part below the heme are shifted to the right in the azole complexes, while the protein part above the heme is moved to the left (Figure 8I, green arrows). The distance between the side chain of Phe163 and Ser263 has to increase to accommodate the azole ring between them, as shown in Figure 8D–F for the example of navoximod (3). This forced opening is smaller in case of the small phenyl azoles binding only to pocket A and larger in case of the fused azole ligands with extensions into pocket B, where additional space needs to be provided for the linker between the A pocket moiety and the B pocket extension (Figure 8D). The aromatic rings of navoximod are roughly perpendicular to the heme plane (green and blue planes in Figure 8F, 84° angle) and point toward the heme propionate group and Gly262 (Figure 8G), not directly toward pocket B. This is different from the indole plane in the cyanide- and *L*-Trp-bound structures (Figure 8H), which is parallel to residues 261–264 and points directly toward the opening of pocket A. It is noticeable that the azole inhibitors with the highest efficiencies (Table S4) are the small inhibitors

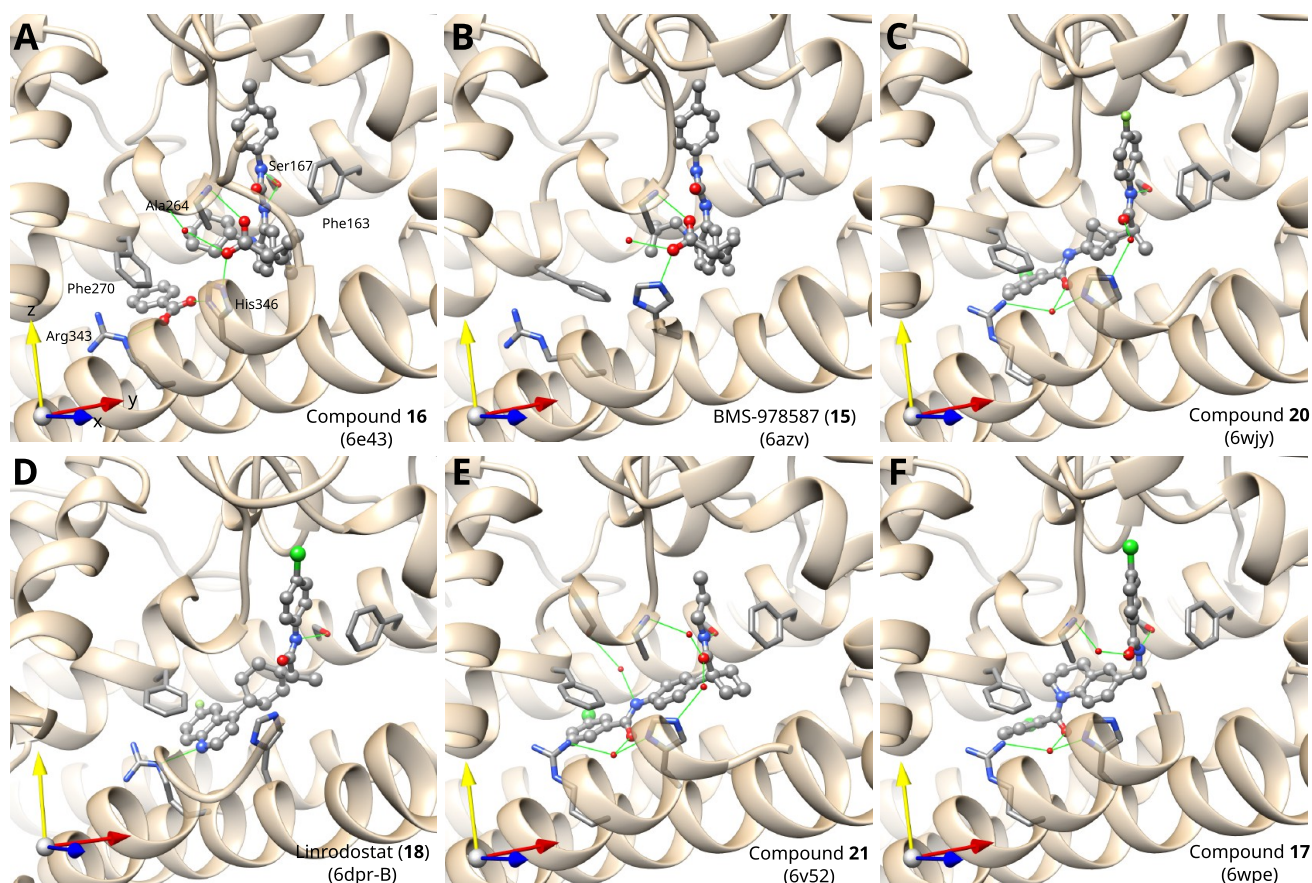


**Figure 10.** Structures of type iv Apo-IDO1 inhibitors. (A) Phenylurea compound **16** (PDB ID 6e43). (B) BMS-978 587 (**15**, PDB ID 6azv). (C) *N*-phenylamide **20** (PDB ID 6wjy). (D) Linrodostat (**18**, PDB ID 6dpr-B). (E) Ligand **21** with an aliphatic A-pocket moiety (PDB ID 6v52). (F) Benzamide **17** (PDB ID 6wpe).

that bind only to pocket A, reaching a high maximal LE of  $-0.80$  kcal/mol (MMG-0752, **10**, PDB ID 7ah6).<sup>65</sup> In comparison, the highest LE reached byazole inhibitors extending into pocket B is significantly lower ( $-0.48$  kcal/mol, compound **2**, PDB ID 5ek4). Even more pronounced than in case of the hydroxamidines, the extension of azoles into pocket B lowers the LE. While these ligands profit from very favorable iron binding energies, they suffer from the drawback that they are not properly oriented to access pocket B. The penalty for this suboptimal complementarity depends on the exact nature and structure of the azoles and can apparently be diminished by fusing the aromatic rings in pocket A, such as in navoximod, the imidazothiazoles, or the indazoles.

A large number of holo-IDO1 inhibitors feature a substituent on the aromatic ring located in pocket A in proximity to Val125, Cys129, Leu234, and Gly262 (Figure 9). This substituent is most often a halogen atom or a methyl group. Some inhibitors feature two halogens, one of which is always a fluorine (Figure 1B).<sup>65</sup> According to their position in pocket A along the *z*-axis, these substituents can roughly be divided into three classes. Larger substituents such as bromide can be located either in a “high position” (Figure 9A) or in a “low position” (Figure 9C). The smaller fluoride substituent preferentially points away from Cys129 and toward the entrance of pocket A (Figure 9B). In many cases, these substituents have been shown to be crucial for increasing the ligand affinity. For example, removing the bromine substituent from MMG-0752 (**10**, PDB ID 7ah6) increases the  $IC_{50}$  value by a factor of 100 from  $0.020$  to  $2 \mu\text{M}$ .<sup>65</sup>

The distance between the halogen substituents and the sulfur atom of Cys129 is often smaller than the sum of their van der Waals radii. However, a halogen bond with Cys129 is only observed in case of the 6-Br-substituted indazoles (Figure 9D).<sup>43</sup> In all other cases, including the 7-Br-substituted indazoles (Figure 9C),<sup>43</sup> the C–halogen...S angle disagrees with a halogen bond, where this angle should be close to  $180^\circ$  due to the  $\sigma$ -hole of the C–halogen bond.<sup>72,73</sup> On the other hand, a “side-on carbon interaction” between the electro-negative belt around halogen atoms and the positively polarized amide carbon of Gly262 is sometimes present.<sup>65</sup> The influence of the sulfur–bromine halogen bond can be estimated from the potencies of the indazole ligands **12** (PDB ID 7e0s) and **13** (PDB ID 7e0t), which differ only in the bromine position. The  $IC_{50}$  value of the ligand with the sulfur–bromine halogen bond is only better by a factor of two ( $0.64$  versus  $1.23 \mu\text{M}$ ).<sup>43</sup> As manifest by the methyl substituent also frequently found in this position, hydrophobic ligand–protein contacts certainly contribute to increasing the binding affinity of substituted ligands. Additionally, the influence of the aromatic substituents on the electronic structure of the heme binding group can modulate the binding affinity.<sup>65</sup>

In summary, the 4-phenylimidazole (**1**)-bound structure (PDB ID 2d0t)<sup>19</sup> has long served for structure-based drug design studies, but it may not reflect the most favorable active site conformation. In all cocrystallized ligands, extensions into pocket B decrease the LE but might be of great importance for modulating other ligand properties. Docking predictions have

proven to be unreliable for capturing the subtle structural effects that penalize B-pocket extensions for azole ligands.

**Apo-IDO1 Type iv Inhibitors.** In 2018, the first two structures of ligand-bound apo-IDO1 were released (PDB IDs 6azv and 6azw),<sup>13</sup> which were soon followed by a structure of improved quality (PDB ID 6e43).<sup>25</sup> To date, there are eight completely heme-free IDO1 structures available (PDB IDs 6azv, 6azw, 6e43, 6v52, 6wjy, 6wpe, 6x5y, and 7m63),<sup>13,25,33,41,47–49</sup> all of which are bound to an inhibitor in the active site (Figure 1C). Additionally, in three structures there is a heme in only one of the two refined protein chains, while the other chain is heme-free (PDB IDs 6dpq-B, 6dpr-B, and 6mq6-B).<sup>33</sup> Based on these intermediate structures, it was concluded that the apo-IDO1 inhibitor linrodostat (**18**) triggers heme release and acts as an irreversible (suicide) inhibitor.<sup>33</sup> However, these conclusions were drawn from a study in a crystalline environment at very high nonphysiological protein and ligand concentrations. Independent detailed cellular and kinetic studies by different groups, on the other hand, suggest that heme binding to IDO1 is reversible under physiological conditions and that a large part of cellular IDO1 is in an apo-form capable of activation by added heme.<sup>13,41,74</sup> Consequently, apo-IDO1 inhibitors also bind reversibly to IDO1, albeit with a very high, sometimes subnanomolar, affinity.

Interestingly, in the structure of a phenylurea ligand (**16**) that does not reach pocket D, the pocket is filled by a benzoate with a high affinity that is kept during the purification steps after bacterial expression (PDB ID 6e43, Figure 10A).<sup>25</sup> Compound **16**, an analogue of the preclinical development candidate BMS-978 587 (**15**),<sup>75</sup> donates hydrogen bonds to Ser167 through the nitrogen atoms of its urea function. It also accepts hydrogen bonds from His346 and the backbone of Ala264 through its carboxylate function. The carboxylate is optimally placed by the cyclopropyl extension of the central phenyl group, which is perpendicular to the heme plane in holo-IDO1. The toluene group fills pocket A, while the two aliphatic substituents of the aniline group extend to the back of the heme binding pocket. The methyl substituent of the toluene group is located in the same site as the halogen and methyl substituents of the holo-IDO1 inhibitors (Figure 9).

Most ligands in the other apo structures are analogues of linrodostat (Figure 10D) with either the same *N*-phenyl-amide scaffold (PDB IDs 6azw, 6dpr, 6mq6, 6wjy) or the inverted benzamide scaffold (PDB IDs 6wpe and 6x5y), which was developed to avoid genotoxicity by the potential metabolic release of 4-chloroaniline.<sup>41</sup> In the *N*-phenyl-amides, the *para*-substituted phenyl ring is bound to pocket A, and the amide nitrogen forms a hydrogen bond with Ser167 (**20**, PDB ID 6wjy). This binding mode superimposes almost perfectly with the position of the *para*-bromo aniline substructure of the type iii inhibitor MMG-0752 (**10**, PDB ID 7ah6), which forms the same hydrogen bond with Ser167 (Supporting Information, Figure S3). The amide oxygen forms a solvent-bridged hydrogen bond to His346. The central part of the ligands is sandwiched between His346 and the back of the heme binding pocket, while the other extremity extends into pocket D. When the D-pocket extension is a quinoline, it forms a hydrogen bond with Arg343 (Figure 10D). In case of the bicyclo[1.1.1]pentane ligand (**20**, PDB ID 6wjy), the phenyl group in pocket D cannot form this hydrogen bond. Instead, an additional amide group participates in a solvent-bridged hydrogen bond network between the ligand and the protein. Ligand **21** shares this motif and binding mode to pocket D (PDB ID 6v52, Figure 10E), although the phenyl

group in pocket A is replaced by a simple aliphatic *n*-propane extension.

In the benzamide scaffold (PDB IDs 6wpe and 6x5y), the *para*-substituted phenyl ring bound to pocket A also forms a hydrogen bond with Ser167 through its amide nitrogen, but the amide oxygen forms a solvent-bridged hydrogen bond to Ser263 instead of His346 (compound **17**, Figure 10F). The central moiety in these ligands is provided by a tetrahydroquinoline moiety located between His346 and Val170. Pocket D is partially filled by an aromatic six-membered ring.

In summary, type iv inhibitors display a very high affinity for IDO1 and have been shown to bind to a physiologically relevant state. They provide a different inhibition mechanism with respect to epacadostat, which has not shown clinical efficacy in the ECHO-301 clinical trial in immuno oncology. Two different classes of type iv inhibitors can be distinguished, namely the phenylureas and the linrodostat analogues. In the second class, a large variety of chemical scaffolds seem to be tolerated.

## SUMMARY AND CONCLUSIONS

In summary, our detailed analysis of the available structural data for IDO1 outlines the plasticity of the active site pockets upon the binding of different ligands. In its ligand-free form, access to pocket A is closed by the movements of residues 261–265. The influence of the heme redox state on the conformation of residues 261–265 is not yet clearly established. In the *L*-Trp substrate-bound state, pocket A opens and JK-loop<sup>C</sup> and Arg231 reorganize to close off the access to the active site, while the solvent and gas channel between helices E and F remains open. Pocket B is severely reduced in size, and pocket C becomes unavailable for ligand binding in the closed JK-loop<sup>C</sup> conformation.

The structural data suggest that pocket D is a secondary binding site for small and predominantly planar ligands in holo-IDO1 and does not bind *L*-Trp. It contradicts the inhibitory binding site hypothesis and the blocked access hypothesis but it is in good agreement with the ordered binding and reduction potential hypothesis based on the modulation of the heme reduction potential by *L*-Trp binding as the source of the observed substrate inhibition at high *L*-Trp concentrations.

Regarding cocrystallized holo-IDO1 inhibitors, our analysis suggests that (i) the heme position and residues 261–265 adapt to the bound ligand, (ii) inhibitors based on heme-bound azoles display a very high ligand efficiency for small ligands but do not allow for direct access to the B pocket due to their preferred orientation, (iii) hydroxyamidine inhibitors allow easier access to the B pocket due to their unique heme-binding conformation, (iv) only few inhibitors with chemical characteristics similar to those of *L*-Trp seem to induce and profit from active site closure by JK-loop<sup>C</sup>, and (v) B-pocket extensions decrease the ligand efficiency but can be beneficial for tuning other ligand properties.

Unfortunately, classical force-field-based modeling tools do not yield the level of detail necessary to describe the energetics of the ligand–heme interactions in the active site, which are very sensitive to the electronic nature of the iron-binding group. An understanding of these energetics and preferred ligand binding conformations necessitates calculations at the quantum mechanical level. As we have demonstrated before, classical docking tools cannot be trusted to predict binding modes and rank activities of different heme-binding groups.<sup>27,28,65,71,76</sup> Here, we extend this observation and suggest that classical docking also fails to predict affinities of azole compounds

extending from pocket A to pocket B, as the intricate dependency on the preferred heme-binding geometry is not captured in these approaches.

## ■ ASSOCIATED CONTENT

### SI Supporting Information

The Supporting Information is available free of charge at <https://pubs.acs.org/doi/10.1021/acs.jmedchem.1c01665>.

X-ray structures of IDO1 and ligands, VHELIBS classifications, holo-IDO1 ligand efficiencies, all chemical structures of cocrystallized IDO1 ligands, additional closed JK-loop<sup>C</sup> structures, superposition of apo- and holo-IDO1 inhibitors, DFT-optimized structures of hydroxyamidinone **5** bound to a heme model, and details of the ESP calculation (PDF)

## ■ AUTHOR INFORMATION

### Corresponding Authors

**Ute F. Röhrig** – Molecular Modeling Group, SIB Swiss Institute of Bioinformatics, CH-1015 Lausanne, Switzerland; [orcid.org/0000-0002-4676-4087](https://orcid.org/0000-0002-4676-4087); Email: [Ute.Roehrig@sib.swiss](mailto:Ute.Roehrig@sib.swiss)

**Olivier Michielin** – Molecular Modeling Group, SIB Swiss Institute of Bioinformatics, CH-1015 Lausanne, Switzerland; Department of Oncology, University Hospital of Lausanne (CHUV), Ludwig Cancer Research—Lausanne Branch, 1011 Lausanne, Switzerland; Email: [Olivier.Michielin@chuv.ch](mailto:Olivier.Michielin@chuv.ch)

**Vincent Zoete** – Molecular Modeling Group, SIB Swiss Institute of Bioinformatics, CH-1015 Lausanne, Switzerland; Department of Oncology UNIL-CHUV, Ludwig Lausanne Branch, 1066 Epalinges, Switzerland; [orcid.org/0000-0002-2336-6537](https://orcid.org/0000-0002-2336-6537); Email: [Vincent.Zoete@unil.ch](mailto:Vincent.Zoete@unil.ch)

Complete contact information is available at: <https://pubs.acs.org/doi/10.1021/acs.jmedchem.1c01665>

### Notes

The authors declare no competing financial interest.

### Biographies

Ute F. Röhrig studied chemistry in Hamburg and Munich with a scholarship from the Studienstiftung des Deutschen Volkes. In 2004, she obtained a Ph.D. degree from the Swiss Federal Institute of Technology Zurich (ETHZ) under the supervision of Ursula Röthlisberger. After a postdoctoral stay in Rome with Roberto Petronzio and Michele Parrinello, Ute F. Röhrig joined the Molecular Modeling Group at the Swiss Institute of Bioinformatics in 2006, where she is presently working as a senior research scientist. She has also been privatdozent at the University of Lausanne since 2016. Her research interests include computational modeling and *in silico* drug design with experimental validation, especially using hybrid quantum and classical methods.

Olivier Michielin is a medical oncologist who specializes in melanoma and precision oncology as well as a bioinformatician involved in the rational design of new cancer therapies. He obtained an Engineer's degree in Physics from the Swiss Federal Institute of Technology Lausanne in 1991, followed by a medical degree from the University of Lausanne in 1997. In 2001, he obtained a M.D.–Ph.D. degree under the supervision of Martin Karplus (2013 Nobel Prize in chemistry) for his work on protein structure–function relationships using molecular simulations. Olivier Michielin obtained his Medical Oncology board certification in 2007. He currently leads the Melanoma Outpatient

Clinic. Olivier Michielin is now full Professor at the Lausanne University Hospital and the Head of the Precision Oncology Center.

Vincent Zoete obtained an Engineer's degree in Chemistry from the ENSCL in 1995, a Master's degree in Drug Design in 1996, and a Ph.D. in Organic Chemistry from the University of Lille in 1999. He did his postdoctoral training in molecular modeling in the groups of Martin Karplus in Strasbourg and Markus Meuwly in Basel. In 2004 he joined the Molecular Modeling Group of the Swiss Institute of Bioinformatics in Lausanne, where he currently is Group Leader. Additionally, he is the scientific director of the Protein Modeling Facility of the University of Lausanne. In 2017, he was appointed Assistant Professor (tenure track) in Molecular Modeling in the Department of Oncology UNIL-CHUV, Ludwig Lausanne Branch. His research interests include the development and application of computer-aided approaches for protein engineering and drug design. He contributed to the development of tools like SwissDock, SwissParam, SwissSide chain, SwissTargetPrediction, SwissSimilarity, SwissBioisostere, and SwissADME.

## ■ ACKNOWLEDGMENTS

We thank Adrià Cereto-Massagué, María José Ojeda, and Gerard Pujadas for providing access to the VHELIBS program and Antoine Daina for providing fruitful discussions. UCSF Chimera<sup>77</sup> was used for displaying, aligning, and analyzing 3D structures. MarvinSketch 20.15 (2020) ChemAxon (<http://www.chemaxon.com>) was used for drawing, displaying, and characterizing chemical structures. ChemAxon is acknowledged for the licensing agreement.

## ■ ABBREVIATIONS USED

ESP, electrostatic potential; IDO, indoleamine 2,3-dioxygenase; LE, ligand efficiency; TDO, tryptophan 2,3-dioxygenase;

## ■ REFERENCES

- (1) Platten, M.; Nollen, E. A. A.; Röhrig, U. F.; Fallarino, F.; Opitz, C. A. Tryptophan metabolism as a common therapeutic target in cancer, neurodegeneration and beyond. *Nat. Rev. Drug Discovery* **2019**, *18*, 379–401.
- (2) Pallotta, M. T.; Rossini, S.; Suvieri, C.; Coletti, A.; Orabona, C.; Macchiarulo, A.; Volpi, C.; Grohmann, U. Indoleamine 2,3-dioxygenase 1 (IDO1): An up-to-date overview of an eclectic immunoregulatory enzyme. *FEBS J.* **2021**, DOI: [10.1111/febs.16086](https://doi.org/10.1111/febs.16086).
- (3) Feng, X.; Liao, D.; Liu, D.; Ping, A.; Li, Z.; Bian, J. Development of indoleamine 2,3-dioxygenase 1 inhibitors for cancer therapy and beyond: A recent perspective. *J. Med. Chem.* **2020**, *63*, 15115–15139.
- (4) Tang, K.; Wu, Y.-H.; Song, Y.; Yu, B. Indoleamine 2,3-dioxygenase 1 (IDO1) inhibitors in clinical trials for cancer immunotherapy. *J. Hematol. Oncol.* **2021**, *14*, 68.
- (5) Long, G. V.; Dummer, R.; Hamid, O.; Gajewski, T. F.; Cagle, C.; Dalle, S.; Arance, A.; Carlino, M. S.; Grob, J.-J.; Kim, T. M.; Demidov, L.; Robert, C.; Larkin, J.; Anderson, J. R.; Maleski, J.; Jones, M.; Diede, S. J.; Mitchell, T. C. Epcadostat plus pembrolizumab versus placebo plus pembrolizumab in patients with unresectable or metastatic melanoma (ECHO-301/KEYNOTE-252): a phase 3, randomised, double-blind study. *Lancet Oncol.* **2019**, *20*, 1083–1097.
- (6) Muller, A. J.; Manfredi, M. G.; Zakharia, Y.; Prendergast, G. C. Inhibiting IDO pathways to treat cancer: lessons from the ECHO-301 trial and beyond. *Semin. Immunopathol.* **2019**, *41*, 41–48.
- (7) Van den Eynde, B. J.; van Baren, N.; Baurain, J.-F. Is there a clinical future for IDO1 inhibitors after the failure of epcadostat in melanoma? *Annu. Rev. Cancer Biol.* **2020**, *4*, 241–256.
- (8) Sonpavde, G.; Necchi, A.; Gupta, S.; Steinberg, G. D.; Gschwend, J. E.; Van Der Heijden, M. S.; Garzon, N.; Ibrahim, M.; Raybold, B.; Liaw, D.; Rutstein, M.; Galsky, M. D. ENERGIIZE: a phase III study of neoadjuvant chemotherapy alone or with nivolumab with/without

linrodostat mesylate for muscle-invasive bladder cancer. *Future Oncol.* **2020**, *16*, 4359–4368.

(9) Kotecki, N.; Vuagnat, P.; O'Neil, B. H.; Jalal, S.; Rottey, S.; Prenen, H.; Benhadji, K. A.; Xia, M.; Szpurka, A. M.; Saha, A.; Wallin, J.; Suriyapperuma, S.; Galvao, V. R.; Geeganage, S.; Doman, T. N.; Gandhi, L.; Xu, X.; Bendell, J. A Phase I Study of an IDO-1 Inhibitor (LY3381916) as Monotherapy and in Combination With an Anti-PD-L1 Antibody (LY3300054) in Patients With Advanced Cancer. *J. Immunother.* **2021**, *44*, 264–275.

(10) Pallotta, M. T.; Orabona, C.; Volpi, C.; Vacca, C.; Belladonna, M. L.; Bianchi, R.; Servillo, G.; Brunacci, C.; Calvitti, M.; Bicciato, S.; Mazza, E. M. C.; Boon, L.; Grassi, F.; Fioretti, M. C.; Fallarino, F.; Puccetti, P.; Grohmann, U. Indoleamine 2,3-dioxygenase is a signaling protein in long-term tolerance by dendritic cells. *Nat. Immunol.* **2011**, *12*, 870–878.

(11) Iacono, A.; Pompa, A.; De Marchis, F.; Panfilii, E.; Greco, F. A.; Coletti, A.; Orabona, C.; Volpi, C.; Belladonna, M. L.; Mondanelli, G.; Albini, E.; Vacca, C.; Gargaro, M.; Fallarino, F.; Bianchi, R.; De Marcos Lousa, C.; Mazza, E. M.; Bicciato, S.; Proietti, E.; Milano, F.; Martelli, M. P.; Iamandii, I. M.; Graupera Garcia-Mila, M.; Lena Sopena, J.; Hawkins, P.; Suire, S.; Okkenhaug, K.; Stark, A.; Grassi, F.; Bellucci, M.; Puccetti, P.; Santambrogio, L.; Macchiarulo, A.; Grohmann, U.; Pallotta, M. T. Class IA PI3Ks regulate subcellular and functional dynamics of IDO1. *EMBO Rep* **2020**, *21*, e49756.

(12) Albini, E.; Rosini, V.; Gargaro, M.; Mondanelli, G.; Belladonna, M. L.; Pallotta, M. T.; Volpi, C.; Fallarino, F.; Macchiarulo, A.; Antognelli, C.; Bianchi, R.; Vacca, C.; Puccetti, P.; Grohmann, U.; Orabona, C. Distinct roles of immunoreceptor tyrosine-based motifs in immunosuppressive indoleamine 2,3-dioxygenase 1. *J. Cell. Mol. Med.* **2017**, *21*, 165–176.

(13) Nelp, M. T.; Kates, P. A.; Hunt, J. T.; Newitt, J. A.; Balog, A.; Maley, D.; Zhu, X.; Abell, L.; Allentoff, A.; Borzilleri, R.; Lewis, H. A.; Lin, Z.; Seitz, S. P.; Yan, C.; Groves, J. T. Immune-modulating enzyme indoleamine 2,3-dioxygenase is effectively inhibited by targeting its apo-form. *Proc. Natl. Acad. Sci. U. S. A.* **2018**, *115*, 3249–3254.

(14) Nelp, M. T.; Zheng, V.; Davis, K. M.; Stiefel, K. J. E.; Groves, J. T. Potent activation of indoleamine 2,3-dioxygenase by polysulfides. *J. Am. Chem. Soc.* **2019**, *141*, 15288–15300.

(15) Lim, Y. J.; Foo, T. C.; Yeung, A. W. S.; Tu, X.; Ma, Y.; Hawkins, C. L.; Witting, P. K.; Jameson, G. N. L.; Terentis, A. C.; Thomas, S. R. Human indoleamine 2,3-dioxygenase 1 is an efficient mammalian nitrite reductase. *Biochemistry* **2019**, *58*, 974–986.

(16) Stanley, C. P.; Maghzal, G. J.; Ayer, A.; Talib, J.; Giltrap, A. M.; Shengule, S.; Wollhuter, K.; Wang, Y.; Chadha, P.; Suarna, C.; Pryszyzhna, O.; Scotcher, J.; Dunn, L. L.; Prado, F. M.; Nguyen, N.; Odiba, J. O.; Baell, J. B.; Stasch, J.-P.; Yamamoto, Y.; Di Mascio, P.; Eaton, P.; Payne, R. J.; Stocker, R. Singlet molecular oxygen regulates vascular tone and blood pressure in inflammation. *Nature* **2019**, *566*, 548–552.

(17) Stanley, C. P.; Stocker, R. Regulation of vascular tone and blood pressure by singlet molecular oxygen in inflammation. *Curr. Opin. Nephrol. Hypertens.* **2021**, *30*, 145–150.

(18) Ju, J.-M.; Nam, G.; Lee, Y.-K.; Jung, M.; Chang, H.; Kim, W.; Shon, W. J.; Lim, J. Y.; Kim, J. Y.; Chang, J.; Min, C. K.; Lee, D.-S.; Choi, K.; Shin, D.-M.; Choi, E. Y. IDO1 scavenges reactive oxygen species in myeloid-derived suppressor cells to prevent graft-versus-host disease. *Proc. Natl. Acad. Sci. U. S. A.* **2021**, *118*, No. e2011170118.

(19) Sugimoto, H.; Oda, S.-I.; Otsuki, T.; Hino, T.; Yoshida, T.; Shiro, Y. Crystal structure of human indoleamine 2,3-dioxygenase: catalytic mechanism of O<sub>2</sub> incorporation by a heme-containing dioxygenase. *Proc. Natl. Acad. Sci. U. S. A.* **2006**, *103*, 2611–2616.

(20) Yue, E. W.; Sparks, R.; Polam, P.; Modi, D.; Douty, B.; Wayland, B.; Glass, B.; Takvorian, A.; Glenn, J.; Zhu, W.; Bower, M.; Liu, X.; Leffet, L.; Wang, Q.; Bowman, K. J.; Hansbury, M. J.; Wei, M.; Li, Y.; Wynn, R.; Burn, T. C.; Koblisch, H. K.; Fridman, J. S.; Emm, T.; Scherle, P. A.; Metcalf, B.; Combs, A. P. INCB24360 (epacadostat), a highly potent and selective indoleamine-2,3-dioxygenase 1 (IDO1) inhibitor for immuno-oncology. *ACS Med. Chem. Lett.* **2017**, *8*, 486–491.

(21) Kumar, S.; Waldo, J. P.; Jaipuri, F. A.; Marcinowicz, A.; Van Allen, C.; Adams, J.; Kesharwani, T.; Zhang, X.; Metz, R.; Oh, A. J.; Harris, S. F.; Mautino, M. R. Discovery of clinical candidate (1R,4R)-4-((R)-2-((S)-6-fluoro-5H-imidazo[5,1-a]isoindol-5-yl)-1-hydroxyethyl)-cyclohexan-1-ol (navoximod), a potent and selective inhibitor of indoleamine 2,3-dioxygenase 1. *J. Med. Chem.* **2019**, *62*, 6705–6733.

(22) Balog, A.; Lin, T.-a.; Maley, D.; Gullo-Brown, J.; Kandoussi, E. H.; Zeng, J.; Hunt, J. T. Preclinical characterization of linrodostat mesylate, a novel, potent, and selective oral indoleamine 2,3-dioxygenase 1 inhibitor. *Mol. Cancer Ther.* **2021**, *20*, 467–476.

(23) Crosignani, S.; Bingham, P.; Botteman, P.; Cannelle, H.; Cauwenberghs, S.; Cordonnier, M.; Dalvie, D.; Deroose, F.; Feng, J. L.; Gomes, B.; Greasley, S.; Kaiser, S. E.; Kraus, M.; Négrerie, M.; Maegley, K.; Miller, N.; Murray, B. W.; Schneider, M.; Solowej, J.; Stewart, A. E.; Tumang, J.; Torti, V. R.; Van Den Eynde, B.; Wythes, M. Discovery of a novel and selective indoleamine 2,3-dioxygenase (IDO-1) inhibitor 3-(5-fluoro-1H-indol-3-yl)pyrrolidine-2,5-dione (EOS200271/PF-06840003) and its characterization as a potential clinical candidate. *J. Med. Chem.* **2017**, *60*, 9617–9629.

(24) Mammoli, A.; Coletti, A.; Ballarotto, M.; Riccio, A.; Carotti, A.; Grohmann, U.; Camaioni, E.; Macchiarulo, A. New insights from crystallographic data: diversity of structural motifs and molecular recognition properties between groups of IDO1 structures. *ChemMedChem* **2020**, *15*, 891–899.

(25) Luo, S.; Xu, K.; Xiang, S.; Chen, J.; Chen, C.; Guo, C.; Tong, Y.; Tong, L. High-resolution structures of inhibitor complexes of human indoleamine 2,3-dioxygenase 1 in a new crystal form. *Acta Crystallogr., Sect. F: Struct. Biol. Commun.* **2018**, *74*, 717–724.

(26) Röhrig, U. F.; Majjigapu, S. R.; Vogel, P.; Zoete, V.; Michielin, O. Challenges in the discovery of indoleamine 2,3-dioxygenase 1 (IDO1) inhibitors. *J. Med. Chem.* **2015**, *58*, 9421–9437.

(27) Röhrig, U. F.; Reynaud, A.; Majjigapu, S. R.; Vogel, P.; Pojer, F.; Zoete, V. Inhibition Mechanisms of Indoleamine 2,3-Dioxygenase 1 (IDO1). *J. Med. Chem.* **2019**, *62*, 8784–8795.

(28) Röhrig, U. F.; Awad, L.; Grosdidier, A.; Larrieu, P.; Stroobant, V.; Colau, D.; Cerundolo, V.; Simpson, A. J. G.; Vogel, P.; Van den Eynde, B. J.; Zoete, V.; Michielin, O. Rational Design of indoleamine 2,3-dioxygenase inhibitors. *J. Med. Chem.* **2010**, *53*, 1172–1189.

(29) Lewis-Ballester, A.; Pham, K. N.; Batabyal, D.; Karkashon, S.; Bonanno, J. B.; Poulos, T. L.; Yeh, S.-R. Structural insights into substrate and inhibitor binding sites in human indoleamine 2,3-dioxygenase 1. *Nat. Commun.* **2017**, *8*, 1693.

(30) Griglio, A.; Torre, E.; Serafini, M.; Bianchi, A.; Schmid, R.; Coda Zabetta, G.; Massarotti, A.; Sorba, G.; Piralì, T.; Fallarini, S. A multicomponent approach in the discovery of indoleamine 2,3-dioxygenase 1 inhibitors: Synthesis, biological investigation and docking studies. *Bioorg. Med. Chem. Lett.* **2018**, *28*, 651–657.

(31) Serafini, M.; Torre, E.; Aprile, S.; Massarotti, A.; Fallarini, S.; Piralì, T. Synthesis, docking and biological evaluation of a novel class of imidazothiazoles as IDO1 inhibitors. *Molecules* **2019**, *24*, 1874.

(32) Serafini, M.; Torre, E.; Aprile, S.; Grosso, E. D.; Gesù, A.; Griglio, A.; Colombo, G.; Travelli, C.; Paiella, S.; Adamo, A.; Orecchini, E.; Coletti, A.; Pallotta, M. T.; Ugel, S.; Massarotti, A.; Piralì, T.; Fallarini, S. Discovery of highly potent benzimidazole derivatives as indoleamine 2,3-dioxygenase-1 (IDO1) inhibitors: from structure-based virtual screening to in vivo pharmacodynamic activity. *J. Med. Chem.* **2020**, *63*, 3047–3065.

(33) Pham, K. N.; Yeh, S.-R. Mapping the binding trajectory of a suicide inhibitor in human indoleamine 2,3-dioxygenase 1. *J. Am. Chem. Soc.* **2018**, *140*, 14538–14541.

(34) Pham, K. N.; Lewis-Ballester, A.; Yeh, S.-R. Conformational plasticity in human heme-based dioxygenases. *J. Am. Chem. Soc.* **2021**, *143*, 1836–1845.

(35) wwPDB consortium. Protein Data Bank: The single global archive for 3D macromolecular structure data. *Nucleic Acids Res.* **2019**, *47*, D520–D528.

(36) Lewis-Ballester, A.; Karkashon, S.; Batabyal, D.; Poulos, T. L.; Yeh, S.-R. Inhibition mechanisms of human indoleamine 2,3-dioxygenase 1. *J. Am. Chem. Soc.* **2018**, *140*, 8518–8525.

- (37) Mirgaux, M.; Leherte, L.; Wouters, J. Influence of the presence of the heme cofactor on the JK-loop structure in indoleamine 2,3-dioxygenase 1. *Acta Crystallogr. Sect. D Struct. Biol.* **2020**, *76*, 1211–1221.
- (38) Tojo, S.; Kohno, T.; Tanaka, T.; Kamioka, S.; Ota, Y.; Ishii, T.; Kamimoto, K.; Asano, S.; Isobe, Y. Crystal structures and structure–activity relationships of imidazothiazole derivatives as IDO1 inhibitors. *ACS Med. Chem. Lett.* **2014**, *5*, 1119–1123.
- (39) Peng, Y.-H.; Ueng, S.-H.; Tseng, C.-T.; Hung, M.-S.; Song, J.-S.; Wu, J.-S.; Liao, F.-Y.; Fan, Y.-S.; Wu, M.-H.; Hsiao, W.-C.; Hsueh, C.-C.; Lin, S.-Y.; Cheng, C.-Y.; Tu, C.-H.; Lee, L.-C.; Cheng, M.-F.; Shia, K.-S.; Shih, C.; Wu, S. Important hydrogen bond networks in indoleamine 2,3-dioxygenase 1 (IDO1) inhibitor design revealed by crystal structures of imidazoleisindole derivatives with IDO1. *J. Med. Chem.* **2016**, *59*, 282–293.
- (40) Peng, Y.-H.; Liao, F.-Y.; Tseng, C.-T.; Kuppusamy, R.; Li, A.-S.; Chen, C.-H.; Fan, Y.-S.; Wang, S.-Y.; Wu, M.-H.; Hsueh, C.-C.; Chang, J.-Y.; Lee, L.-C.; Shih, C.; Shia, K.-S.; Yeh, T.-K.; Hung, M.-S.; Kuo, C.-C.; Song, J.-S.; Wu, S.-Y.; Ueng, S.-H. Unique Sulfur–Aromatic Interactions Contribute to the Binding of Potent Imidazothiazole Indoleamine 2,3-Dioxygenase Inhibitors. *J. Med. Chem.* **2020**, *63*, 1642–1659.
- (41) Hamilton, M. M.; Mseeh, F.; McAfoos, T. J.; Leonard, P. G.; Reyna, N. J.; Harris, A. L.; Xu, A.; Han, M.; Soth, M. J.; Czado, B.; Theroff, J. P.; Mandal, P. K.; Burke, J. P.; Virgin-Downey, B.; Petrocchi, A.; Pfaffinger, D.; Rogers, N. E.; Parker, C. A.; Yu, S. S.; Jiang, Y.; Krapp, S.; Lammens, A.; Trevitt, G.; Tremblay, M. R.; Mikule, K.; Wilcoxon, K.; Cross, J. B.; Jones, P.; Marszalek, J. R.; Lewis, R. T. Discovery of IACS-9779 and IACS-70465as potent inhibitors targeting indoleamine 2,3-dioxygenase 1 (IDO1) apoenzyme. *J. Med. Chem.* **2021**, *64*, 11302–11329.
- (42) Alexandre, J. A. C.; Swan, M. K.; Latchem, M. J.; Boyall, D.; Pollard, J. R.; Hughes, S. W.; Westcott, J. New 4-amino-1,2,3-triazole inhibitors of indoleamine 2,3-dioxygenase form a long-lived complex with the enzyme and display exquisite cellular potency. *ChemBioChem* **2018**, *19*, 552–561.
- (43) Ning, X.-L.; Li, Y.-Z.; Huo, C.; Deng, J.; Gao, C.; Zhu, K.-R.; Wang, M.; Wu, Y.-X.; Yu, J.-L.; Ren, Y.-L.; Luo, Z.-Y.; Li, G.; Chen, Y.; Wang, S.-Y.; Peng, C.; Yang, L.-L.; Wang, Z.-Y.; Wu, Y.; Qian, S.; Li, G.-B. X-ray structure-guided discovery of a potent, orally bioavailable, dual human indoleamine/tryptophan 2,3-dioxygenase (hIDO/hTDO) inhibitor that shows activity in a mouse model of parkinson's disease. *J. Med. Chem.* **2021**, *64*, 8303–8332.
- (44) Wu, Y.; Xu, T.; Liu, J.; Ding, K.; Xu, J. Structural insights into the binding mechanism of IDO1 with hydroxylamide based inhibitor INCB14943. *Biochem. Biophys. Res. Commun.* **2017**, *487*, 339–343.
- (45) Zhang, H.; Liu, K.; Pu, Q.; Achab, A.; Ardolino, M. J.; Cheng, M.; Deng, Y.; Doty, A. C.; Ferguson, H.; Fradera, X.; Knemeyer, I.; Kurukulasuriya, R.; Lam, Y. H.; Lesburg, C. A.; Martinot, T. A.; McGowan, M. A.; Miller, J. R.; Otte, K.; Biju, P. J.; Sciammetta, N.; Solban, N.; Yu, W.; Zhou, H.; Wang, X.; Bennett, D. J.; Han, Y. Discovery of amino-cyclobutane-derived indoleamine-2,3-dioxygenase 1 (IDO1) inhibitors for cancer immunotherapy. *ACS Med. Chem. Lett.* **2019**, *10*, 1530–1536.
- (46) Pham, K. N.; Lewis-Ballester, A.; Yeh, S.-r. Structural basis of inhibitor selectivity in human indoleamine 2,3-dioxygenase 1 and tryptophan dioxygenase. *J. Am. Chem. Soc.* **2019**, *141*, 18771–18779.
- (47) White, C.; McGowan, M. A.; Zhou, H.; Sciammetta, N.; Fradera, X.; Lim, J.; Joshi, E. M.; Andrews, C.; Nickbarg, E. B.; Cowley, P.; Trewick, S.; Augustin, M.; von Koenig, K.; Lesburg, C. A.; Otte, K.; Knemeyer, I.; Woo, H.; Yu, W.; Cheng, M.; Spacciapoli, P.; Geda, P.; Song, X.; Smotrov, N.; Curran, P.; Heo, M. R.; Abeywickrema, P.; Miller, J. R.; Bennett, D. J.; Han, Y. Strategic incorporation of polarity in heme-displacing inhibitors of indoleamine-2,3-dioxygenase-1 (IDO1). *ACS Med. Chem. Lett.* **2020**, *11*, 550–557.
- (48) Pu, Q.; Zhang, H.; Guo, L.; Cheng, M.; Doty, A. C.; Ferguson, H.; Fradera, X.; Lesburg, C. A.; McGowan, M. A.; Miller, J. R.; Geda, P.; Song, X.; Otte, K.; Sciammetta, N.; Solban, N.; Yu, W.; Sloman, D. L.; Zhou, H.; Lammens, A.; Neumann, L.; Bennett, D. J.; Pasternak, A.; Han, Y. Discovery of potent and orally available bicyclo[1.1.1]pentane-derived indoleamine-2,3-dioxygenase 1 (IDO1) inhibitors. *ACS Med. Chem. Lett.* **2020**, *11*, 1548–1554.
- (49) Li, D.; Deng, Y.; Achab, A.; Bharathan, I.; Hopkins, B. A.; Yu, W.; Zhang, H.; Sanyal, S.; Pu, Q.; Zhou, H.; Liu, K.; Lim, J.; Fradera, X.; Lesburg, C. A.; Lammens, A.; Martinot, T. A.; Cohen, R. D.; Doty, A. C.; Ferguson, H.; Nickbarg, E. B.; Cheng, M.; Spacciapoli, P.; Geda, P.; Song, X.; Smotrov, N.; Abeywickrema, P.; Andrews, C.; Chamberlin, C.; Mabrouk, O.; Curran, P.; Richards, M.; Saradjian, P.; Miller, J. R.; Knemeyer, I.; Otte, K. M.; Vincent, S.; Sciammetta, N.; Pasternak, A.; Bennett, D. J.; Han, Y. Carbamate and N-pyrimidine mitigate amide hydrolysis: structure-based drug design of tetrahydroquinoline IDO1 inhibitors. *ACS Med. Chem. Lett.* **2021**, *12*, 389–396.
- (50) Hopkins, B.; Zhang, H.; Bharathan, I.; Li, D.; Pu, Q.; Zhou, H.; Martinot, T. A.; Fradera, X.; Lammens, A.; Lesburg, C. A.; Cohen, R. D.; Ballard, J.; Knemeyer, I.; Otte, K.; Vincent, S.; Miller, J. R.; Solban, N.; Cheng, M.; Geda, P.; Smotrov, N.; Song, X.; Bennett, D. J.; Han, Y. Utilization of Metabolite Identification and Structural Data to Guide Design of Low-Dose IDO1 Inhibitors. *ACS Med. Chem. Lett.* **2021**, *12*, 1435–1440.
- (51) Forouhar, F.; Anderson, J. L. R.; Mowat, C. G.; Vorobiev, S. M.; Hussain, A.; Abashidze, M.; Bruckmann, C.; Thackray, S. J.; Seetharaman, J.; Tucker, T.; Xiao, R.; Ma, L.-c.; Zhao, L.; Acton, T. B.; Montelione, G. T.; Chapman, S. K.; Tong, L. Molecular insights into substrate recognition and catalysis by tryptophan 2,3-dioxygenase. *Proc. Natl. Acad. Sci. U. S. A.* **2007**, *104*, 473–8.
- (52) Read, R. J.; Adams, P. D.; Arendall, W. B.; Brunger, A. T.; Emsley, P.; Joosten, R. P.; Kleywegt, G. J.; Krissinel, E. B.; Lütke, T.; Otwinowski, Z.; Perrakis, A.; Richardson, J. S.; Sheffler, W. H.; Smith, J. L.; Tickle, I. J.; Vriend, G.; Zwart, P. H. A new generation of crystallographic validation tools for the protein data bank. *Structure* **2011**, *19*, 1395–1412.
- (53) Gore, S.; Sanz García, E.; Hendrickx, P. M.; Gutmanas, A.; Westbrook, J. D.; Yang, H.; Feng, Z.; Baskaran, K.; Berrisford, J. M.; Hudson, B. P.; Ikegawa, Y.; Kobayashi, N.; Lawson, C. L.; Mading, S.; Mak, L.; Mukhopadhyay, A.; Oldfield, T. J.; Patwardhan, A.; Peisach, E.; Sahni, G.; Sekharan, M. R.; Sen, S.; Shao, C.; Smart, O. S.; Ulrich, E. L.; Yamashita, R.; Quesada, M.; Young, J. Y.; Nakamura, H.; Markley, J. L.; Berman, H. M.; Burley, S. K.; Velankar, S.; Kleywegt, G. J. Validation of structures in the protein data bank. *Structure* **2017**, *25*, 1916–1927.
- (54) Blow, D. M. Rearrangement of Cruickshank's formulae for the diffraction-component precision index. *Acta Crystallogr., Sect. D: Biol. Crystallogr.* **2002**, *58*, 792–797.
- (55) Goto, J.; Kataoka, R.; Hirayama, N. Ph4Dock: Pharmacophore-based protein–ligand docking. *J. Med. Chem.* **2004**, *47*, 6804–6811.
- (56) Cereto-Massagué, A.; Ojeda, M. J.; Joosten, R. P.; Valls, C.; Mulero, M.; Salvado, M. J.; Arola-Arnal, A.; Arola, L.; Garcia-Vallvé, S.; Pujadas, G. The good, the bad and the dubious: VHELIBS, a validation helper for ligands and binding sites. *J. Cheminform.* **2013**, *5*, 36.
- (57) Meyder, A.; Nittinger, E.; Lange, G.; Klein, R.; Rarey, M. Estimating electron density support for individual atoms and molecular fragments in X-ray structures. *J. Chem. Inf. Model.* **2017**, *57*, 2437–2447.
- (58) Álvarez, L.; Lewis-Ballester, A.; Roitberg, A.; Estrin, D. A.; Yeh, S.-R.; Marti, M. A.; Capece, L. Structural study of a flexible active site loop in human indoleamine 2,3-dioxygenase and its functional implications. *Biochemistry* **2016**, *55*, 2785–2793.
- (59) Yamamoto, S.; Hayaishi, O. Tryptophan pyrrolase of rabbit intestine. D- and L-tryptophan-cleaving enzyme or enzymes. *J. Biol. Chem.* **1967**, *242*, 5260–5266.
- (60) Sono, M.; Taniguchi, T.; Watanabe, Y.; Hayaishi, O. Indoleamine 2,3-dioxygenase. Equilibrium studies of the tryptophan binding to the ferric, ferrous, and CO-bound enzymes. *J. Biol. Chem.* **1980**, *255*, 1339–1345.
- (61) Lu, C.; Lin, Y.; Yeh, S.-r. Inhibitory substrate binding site of human indoleamine 2,3-dioxygenase. *J. Am. Chem. Soc.* **2009**, *131*, 12866–12867.

(62) Nickel, E.; Nienhaus, K.; Lu, C.; Yeh, S.-r.; Nienhaus, G. U. Ligand and substrate migration in human indoleamine 2,3-dioxygenase. *J. Biol. Chem.* **2009**, *284*, 31548–31554.

(63) Lu, C.; Lin, Y.; Yeh, S.-r. Spectroscopic studies of ligand and substrate binding to human indoleamine 2,3-dioxygenase. *Biochemistry* **2010**, *49*, 5028–5034.

(64) Nienhaus, K.; Nickel, E.; Lu, C.; Yeh, S.-r.; Nienhaus, G. U. Ligand migration in human indoleamine-2,3 dioxygenase. *IUBMB Life* **2011**, *63*, 153–159.

(65) Röhrig, U. F.; Majjigapu, S. R.; Reynaud, A.; Pojer, F.; Dilek, N.; Reichenbach, P.; Ascencao, K.; Irving, M.; Coukos, G.; Vogel, P.; Michielin, O.; Zoete, V. Azole-based indoleamine 2,3-dioxygenase 1 (IDO1) inhibitors. *J. Med. Chem.* **2021**, *64*, 2205–2227.

(66) Weber, B.; Nickel, E.; Horn, M.; Nienhaus, K.; Nienhaus, G. U. Substrate inhibition in human indoleamine 2,3-dioxygenase. *J. Phys. Chem. Lett.* **2014**, *5*, 756–761.

(67) Kolawole, A. O.; Hixon, B. P.; Dameron, L. S.; Chrisman, I. M.; Smirnov, V. V. Catalytic activity of human indoleamine 2,3-dioxygenase (hIDO1) at low oxygen. *Arch. Biochem. Biophys.* **2015**, *570*, 47–57.

(68) Efimov, I.; Basran, J.; Sun, X.; Chauhan, N.; Chapman, S. K.; Mowat, C. G.; Raven, E. L. The mechanism of substrate inhibition in human indoleamine 2,3-dioxygenase. *J. Am. Chem. Soc.* **2012**, *134*, 3034–3041.

(69) Terentis, A. C.; Thomas, S. R.; Takikawa, O.; Littlejohn, T. K.; Truscott, R. J. W.; Armstrong, R. S.; Yeh, S.-r.; Stocker, R. The heme environment of recombinant human indoleamine 2,3-dioxygenase. Structural properties and substrate-ligand interactions. *J. Biol. Chem.* **2002**, *277*, 15788–15794.

(70) Yue, E. W.; Douty, B.; Wayland, B.; Bower, M.; Liu, X.; Leffet, L.; Wang, Q.; Bowman, K. J.; Hansbury, M. J.; Liu, C.; Wei, M.; Li, Y.; Wynn, R.; Burn, T. C.; Koblisch, H. K.; Fridman, J. S.; Metcalf, B.; Scherle, P. A.; Combs, A. P. Discovery of potent competitive inhibitors of indoleamine 2,3-dioxygenase with in vivo pharmacodynamic activity and efficacy in a mouse melanoma model. *J. Med. Chem.* **2009**, *52*, 7364–7367.

(71) Röhrig, U. F.; Zoete, V.; Michielin, O. The binding mode of N-hydroxyamidines to indoleamine 2,3-dioxygenase 1 (IDO1). *Biochemistry* **2017**, *56*, 4323–4325.

(72) Wilcken, R.; Zimmermann, M. O.; Lange, A.; Zahn, S.; Kirchner, B.; Boeckler, F. M. Addressing methionine in molecular design through directed sulfur–halogen bonds. *J. Chem. Theory Comput.* **2011**, *7*, 2307–2315.

(73) Wilcken, R.; Zimmermann, M. O.; Lange, A.; Joerger, A. C.; Boeckler, F. M. Principles and applications of halogen bonding in medicinal chemistry and chemical biology. *J. Med. Chem.* **2013**, *56*, 1363–1388.

(74) Ortiz-Meoz, R. F.; Wang, L.; Matico, R.; Rutkowska-Klute, A.; De la Rosa, M.; Bedard, S.; Midgett, R.; Strohmmer, K.; Thomson, D.; Zhang, C.; Mebrahtu, M.; Guss, J.; Totoritis, R.; Consler, T.; Campobasso, N.; Taylor, D.; Lewis, T.; Weaver, K.; Muelbaier, M.; Seal, J.; Dunham, R.; Kazmierski, W.; Favre, D.; Bergamini, G.; Shewchuk, L.; Rendina, A.; Zhang, G. Characterization of apo-form selective inhibition of indoleamine 2,3-dioxygenase. *ChemBioChem* **2021**, *22*, 516–522.

(75) Maity, P.; Reddy, V. V. R.; Mohan, J.; Korapati, S.; Narayana, H.; Cherupally, N.; Chandrasekaran, S.; Ramachandran, R.; Sfougatakis, C.; Eastgate, M. D.; Simmons, E. M.; Vaidyanathan, R. Development of a scalable synthesis of BMS-978587 featuring a stereospecific suzuki coupling of a cyclopropane carboxylic acid. *Org. Process Res. Dev.* **2018**, *22*, 888–897.

(76) Röhrig, U. F.; Majjigapu, S. R.; Grosdidier, A.; Bron, S.; Stroobant, V.; Pilotte, L.; Colau, D.; Vogel, P.; Van den Eynde, B. J.; Zoete, V.; Michielin, O. Rational design of 4-aryl-1,2,3-triazoles for indoleamine 2,3-dioxygenase 1 inhibition. *J. Med. Chem.* **2012**, *55*, 5270–5290.

(77) Pettersen, E. F.; Goddard, T. D.; Huang, C. C.; Couch, G. S.; Greenblatt, D. M.; Meng, E. C.; Ferrin, T. E. UCSF Chimera—A visualization system for exploratory research and analysis. *J. Comput. Chem.* **2004**, *25*, 1605–1612.

## Recommended by ACS

### Discovery of CH7057288 as an Orally Bioavailable, Selective, and Potent pan-TRK Inhibitor

Toshiya Ito, Nobuhiro Oikawa, *et al.*

SEPTEMBER 06, 2022  
JOURNAL OF MEDICINAL CHEMISTRY

READ 

### Venglustat Inhibits Protein N-Terminal Methyltransferase 1 in a Substrate-Competitive Manner

Guangping Dong, Rong Huang, *et al.*

SEPTEMBER 08, 2022  
JOURNAL OF MEDICINAL CHEMISTRY

READ 

### Development of Selective Phosphatidylinositol 5-Phosphate 4-Kinase $\gamma$ Inhibitors with a Non-ATP-competitive, Allosteric Binding Mode

Helen K. Boffey, Stephen P. Andrews, *et al.*

FEBRUARY 11, 2022  
JOURNAL OF MEDICINAL CHEMISTRY

READ 

### Discovery of a Potent and Selective ATAD2 Bromodomain Inhibitor with Antiproliferative Activity in Breast Cancer Models

Jon J. Winter-Holt, Sylvie Guichard, *et al.*

FEBRUARY 08, 2022  
JOURNAL OF MEDICINAL CHEMISTRY

READ 

Get More Suggestions >